Supporting information for

Synthesis and Optical Properties of N→Ga Coordinated Galliumboroxines†

Yaraslava Milasheuskaya,[a] Jiří Schwarz,[a] Libor Dostál,[a] Zdenka Růžičková,[a] Marek Bouška,[b] Zuzana Olmrová Zmrhalová,[c] Tomáš Syrový,[b] Roman Jambor[a]*

[a] Department of General and Inorganic Chemistry, University of Pardubice, 532 10 Pardubice, Czech Republic, E-mail: roman.jambor@upce.cz,

[b] Department of Graphic Arts and Photophysics, Faculty of Chemical Technology, University of Pardubice, 532 10 Pardubice, Czech Republic

[c] Center of Materials and Nanotechnologies, Faculty of Chemical Technology, University of Pardubice, 532 10 Pardubice, Czech Republic

Contents:

Result and Discussion

Electrical conductivity measurements p. S2

Supramolecular architecture p. S3

Figures S2 – S44 p. S4 – p. S47

Tables S1 – S6 p. S48 – p. S51

Literature p. S52

Result and Discussion

Electrical conductivity measurements

Besides the optical properties that match with those found for Ga doped borate glasses, the specific surface conductivity of the thin films of **5** was also measured to determine the activation energy of surface electrical conductivity (E_a^s) and pre-exponential factor (σ_0) (Figure S1, Table 2). The dependence of specific surface conductivity on the temperature was measured in the range of 100 – 200 °C, where no degradation of **5** was observed by the help of the graphite electrode (Figure S39). The temperature dependence of the electrical conductivity is similar for both layers and contrasts to the SiO_2 substrate. The values of σ_0, which depend on the chemical composition, are generally in several order of magnitude.[S1] In our case, a significant difference of σ_0 between the prepared layers of **5** (σ_0 = 86 and 9 S) and the substrate ($\sigma_0 = 8 \cdot 10^{-5}$ S) is also evident. The values of E_a^s were determined by the interpolation of the above temperature dependences using the Arrhenius equation.

$$\sigma = \sigma_0 e^{-E_a^s/RT}$$

The values of E_a^s (0.992 and 0.907 eV) determined for thin layer of **5** are also close to the manganese-borate and sodium-borate glass with E_a^s = 1.0 – 1.7 eV.[S2]

The supramolecular architecture

We have found differences in the supramolecular architecture of GBOs **2** – **6**. While compounds **3**, **4** and **6** did not reveal notable intermolecular contacts, these were observed in **2** and **5**. In the case of **2**, the central GaB_2O_3 ring is connected by O1-H·····B2a (3.486(3) Å), B1·····H-O3a (3.548(3) Å), B2·····H-O1b (3.486(3) Å), and O3-H·····B1b (3.548(3) Å) interactions, respectively, to provide 1D infinitive chain. The latter is connected by the interactions of the C*H*$_2$N hydrogens with the B*O*H and B_2*O* oxygen atoms [interactions of C5-H·····O5c (3.626(3) Å) and C5-H·····O2c (3.325(3) Å), respectively] (see Figure S7a) to give a 2D arrangement of **2** (for view along axis a or c see Figures S7b, c). All these weak contacts, however, did not result in the pyramidalization at the boron atoms. In contrast, no O·····B interactions are in **5**, but the methyl NC*H*$_3$ hydrogens of the ligand L interact with oxygen atoms of the C(H)*O* group [interactions C7-H·····O3a(b) (3.137(2) Å) and O3·····H-C7a(b) (3.137(2) Å), respectively] (see Figure 8a) to provide 1D infinitive chain in **5** (for view along axis a or c see Figures S8b,c).

Figure S1. The temperature dependence of specific surface conductivity for thin films of **5**.

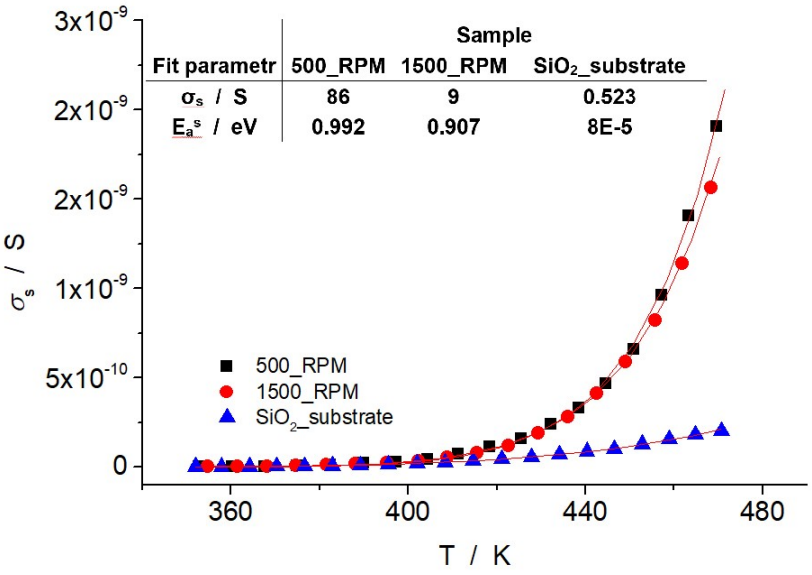

Figure S2. ORTEP plot of a molecule of **2** showing 30% probability displacement ellipsoid. Hydrogen atoms are omitted for clarity

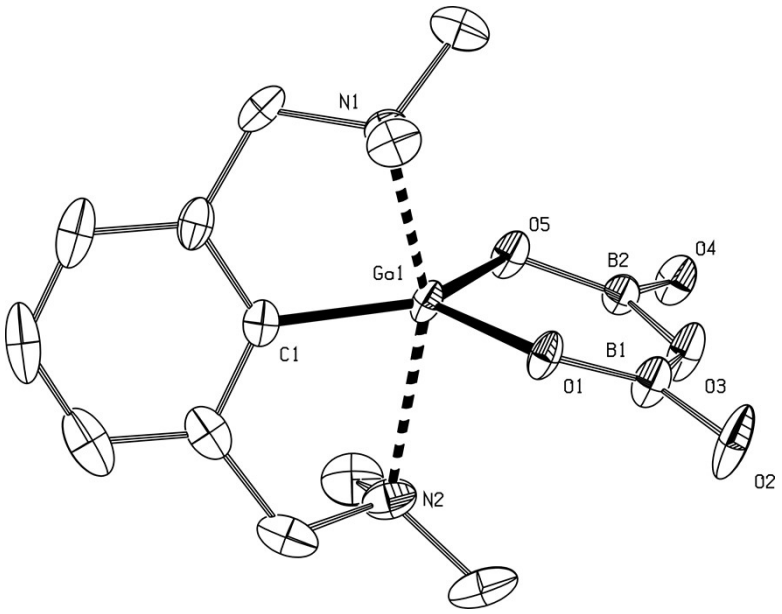

Figure S3. ORTEP plot of a molecule of **3** showing 30% probability displacement ellipsoid. Hydrogen atoms are omitted for clarity

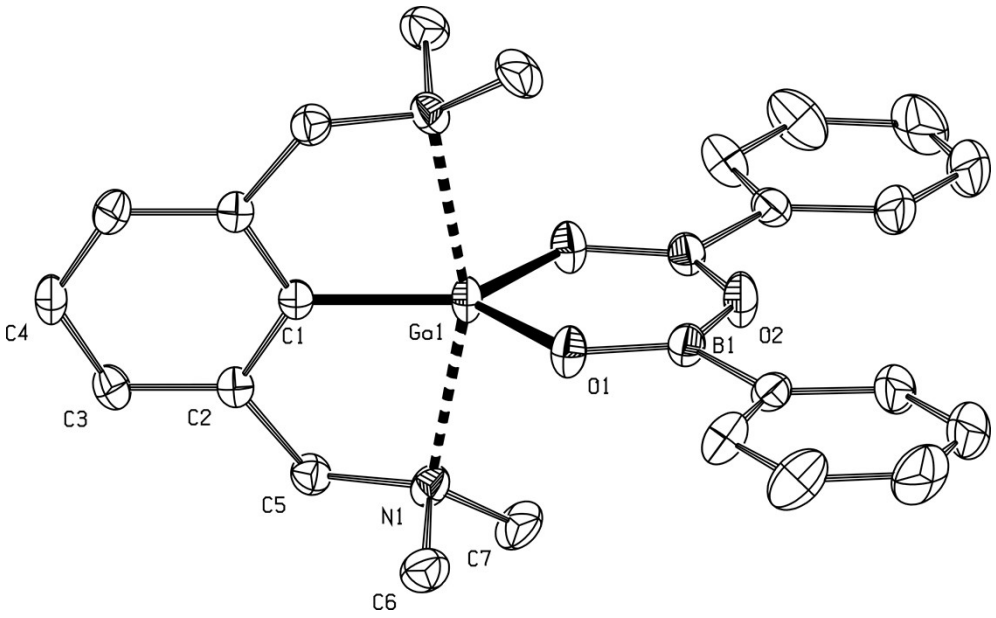

Figure S4. ORTEP plot of a molecule of **4** showing 30% probability displacement ellipsoid. Hydrogen atoms are omitted for clarity

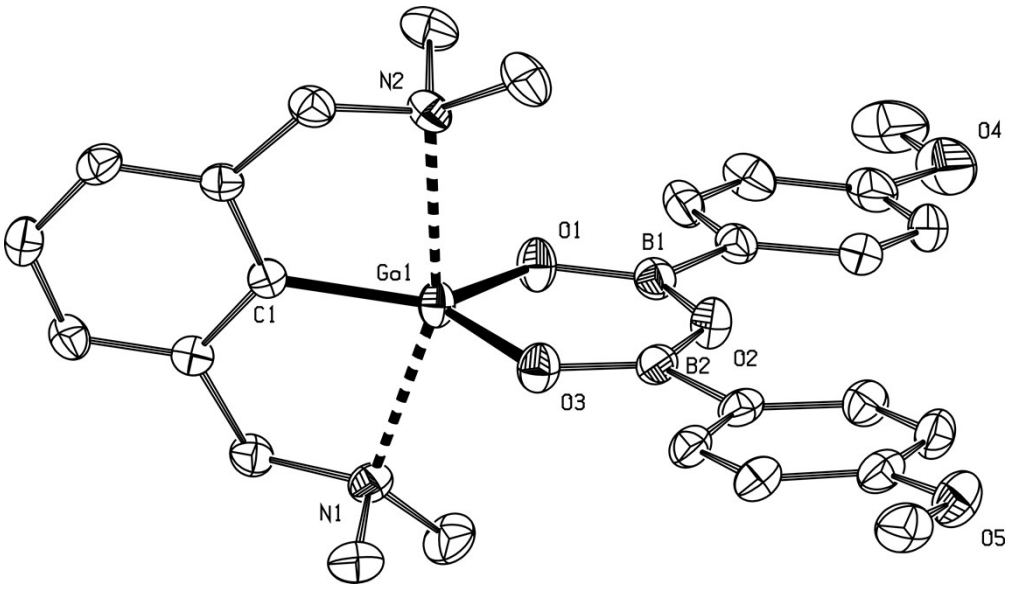

Figure S5. ORTEP plot of a molecule of **5** showing 30% probability displacement ellipsoid. Hydrogen atoms are omitted for clarity

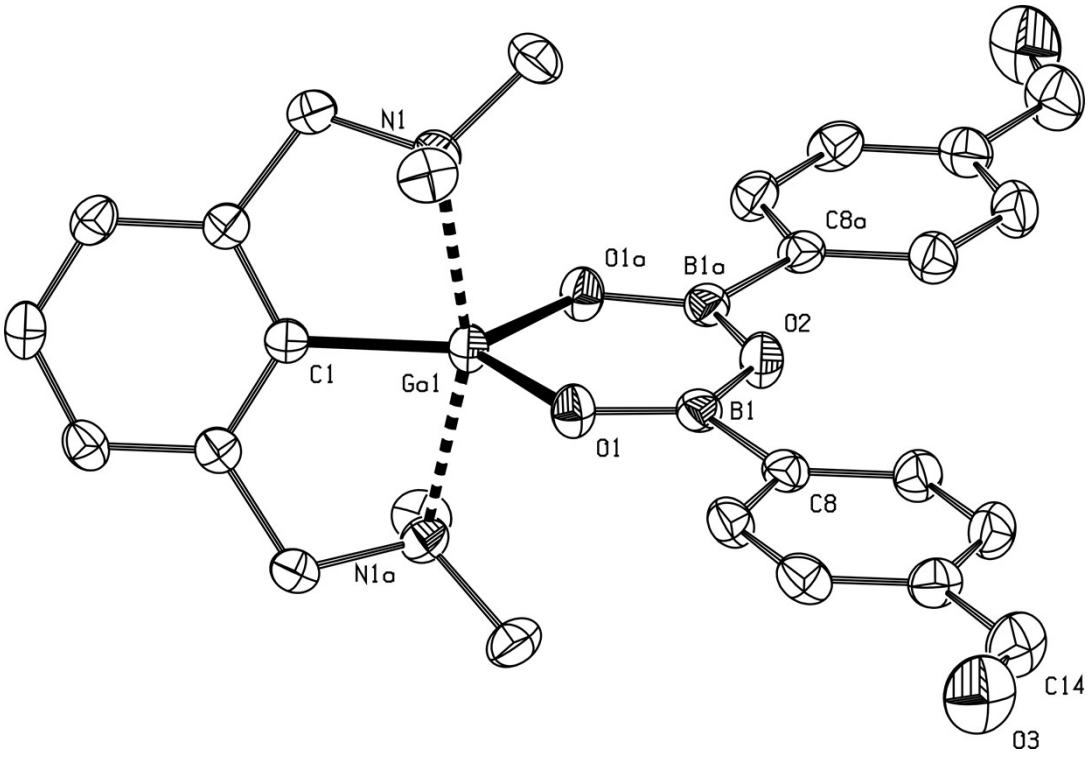

Figure S6. ORTEP plot of a molecule of **6** showing 30% probability displacement ellipsoid. Hydrogen atoms are omitted for clarity

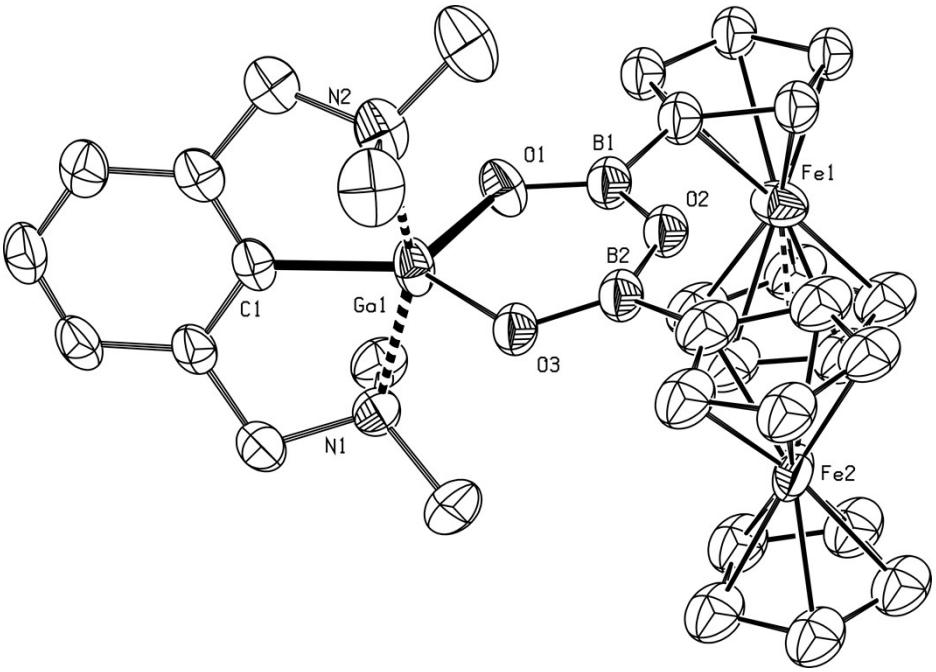

Figure S7. Supramolecular architecture of GBO **2.** Intermolecular contacts of the central GaB_2O_3 ring (**A**) together with the view along the axis a (B) and c (C).

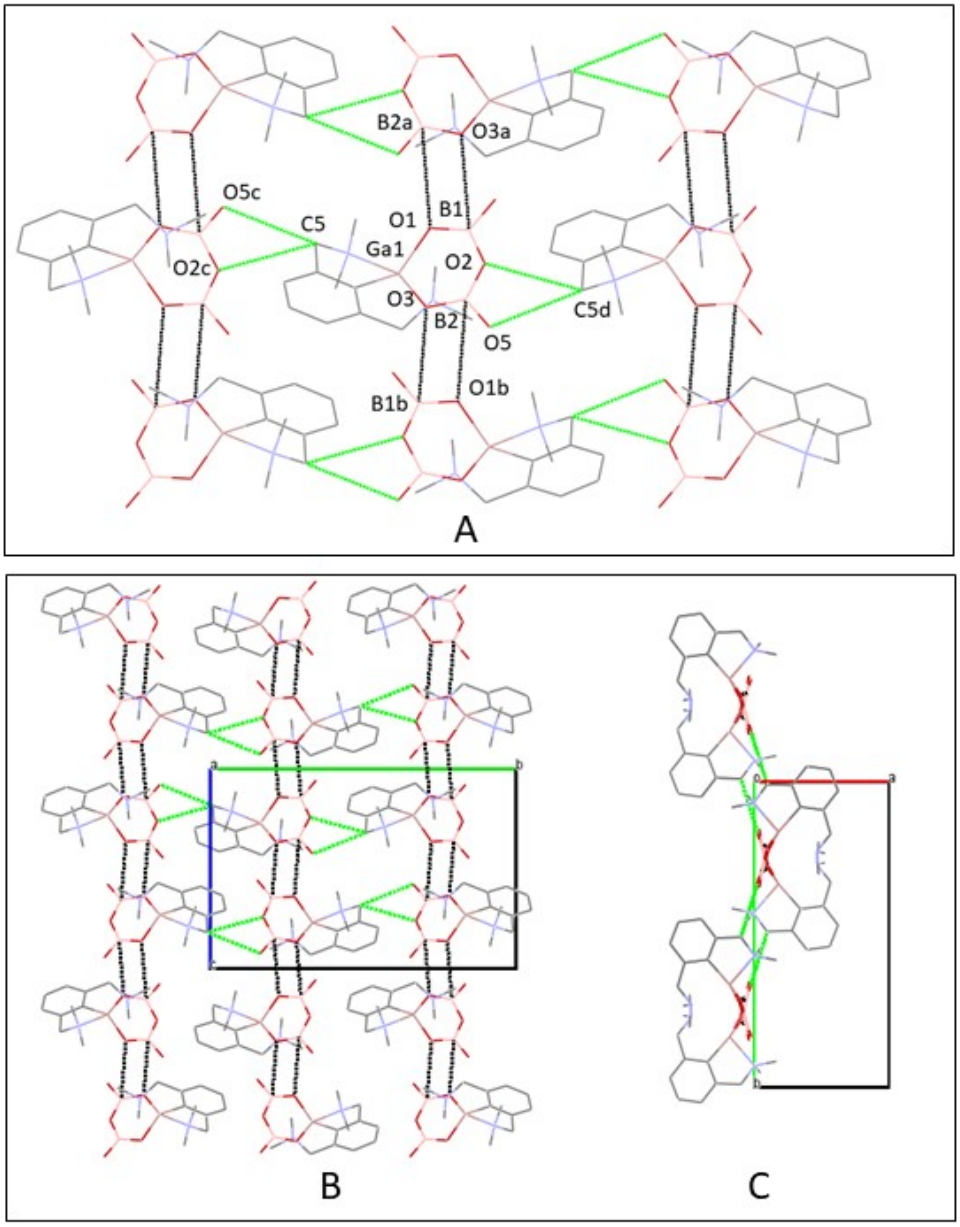

Figure S8. Supramolecular architecture of GBO **5.** Intermolecular contacts found in GBO **5** (**A**) together with the view along the axis a (B) and c (C).

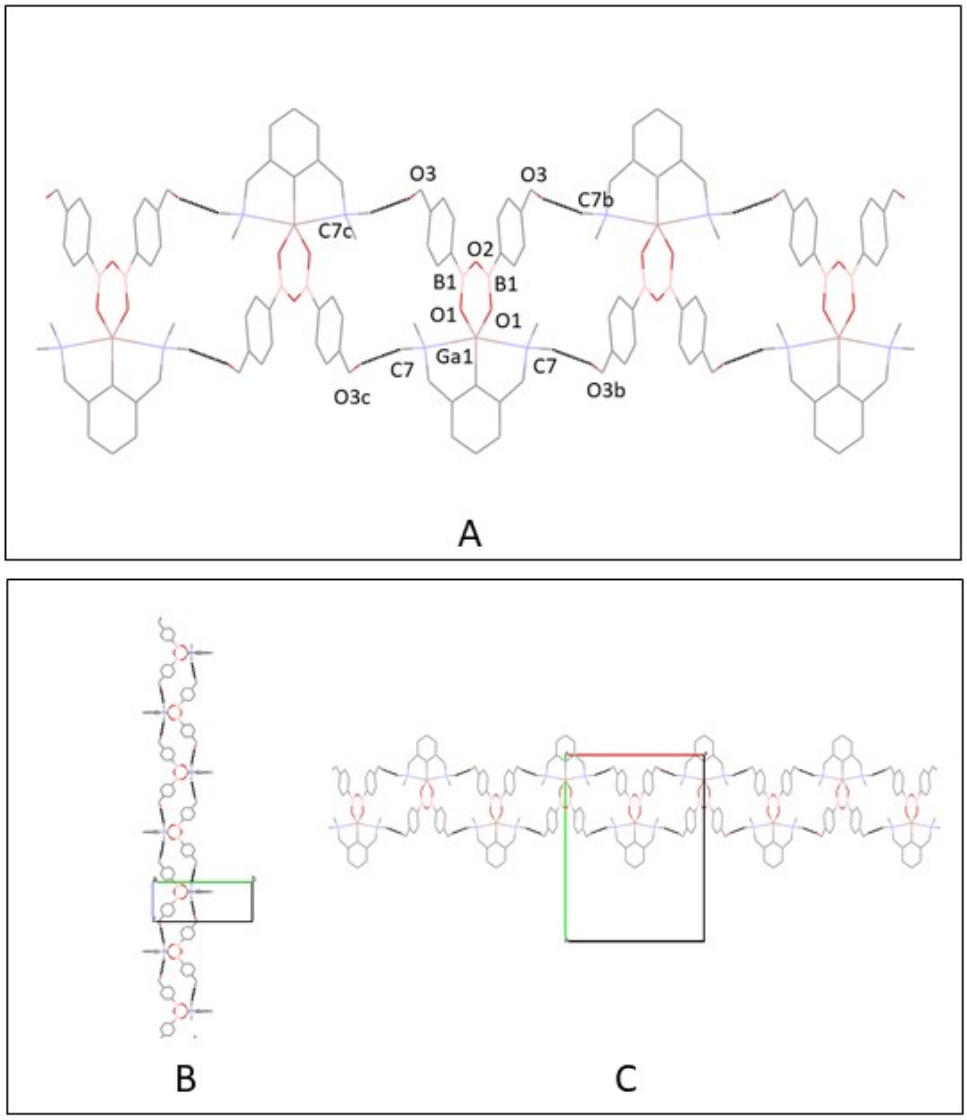

Figure S9. ^{1}H NMR (500.20 MHz, $CDCl_3$, 300 K) of compound **2**

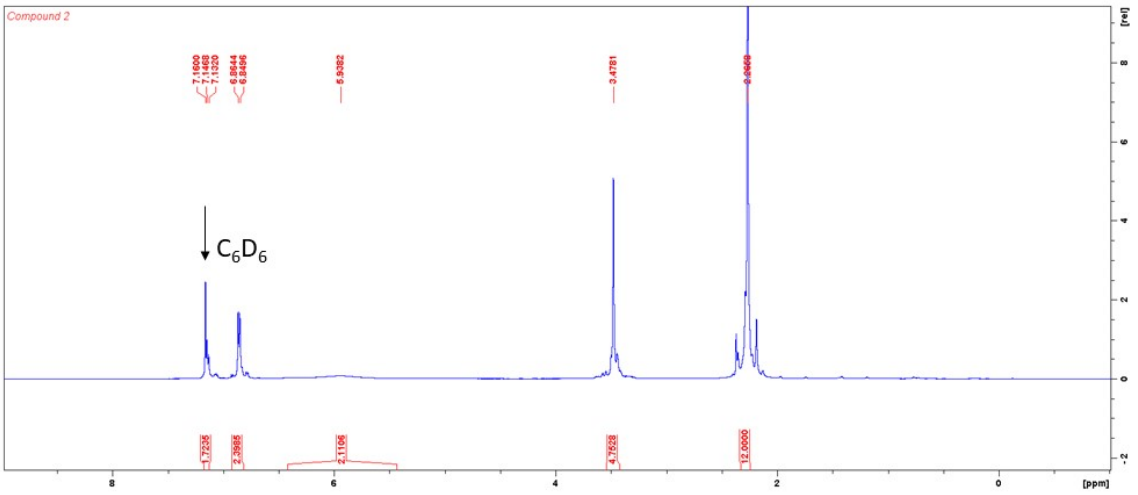

Figure S10. $^{13}C\{^{1}H\}$ NMR APT spectrum (125.78 MHz, $CDCl_3$, 300 K) of compound **2**

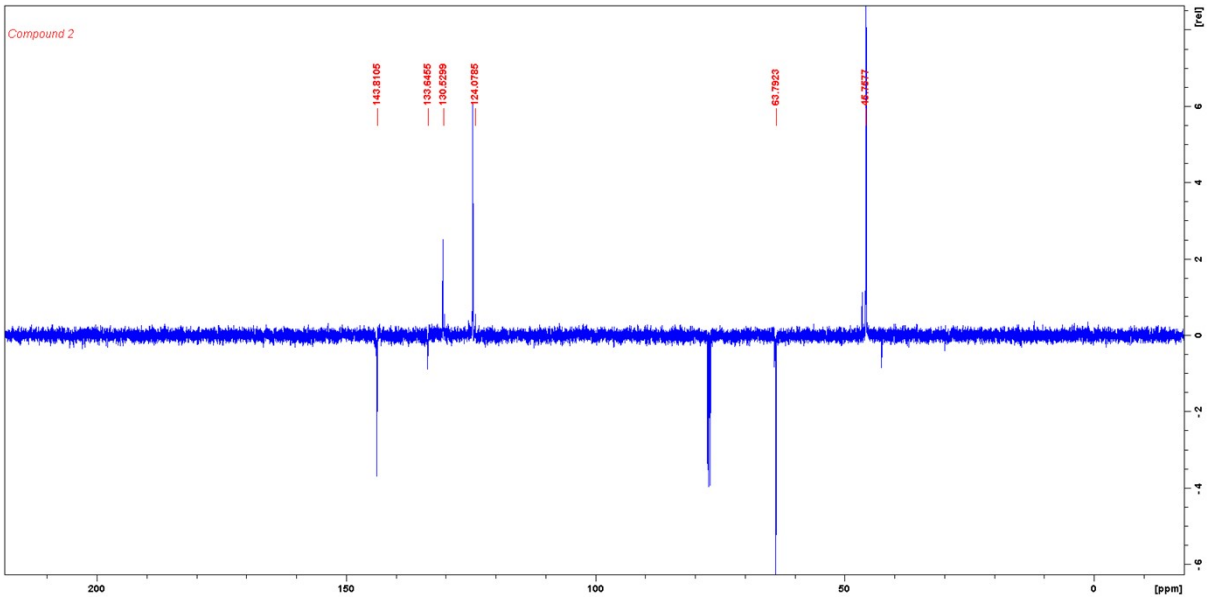

Figure S11. $^{11}B\{^{1}H\}$ NMR (160.49 MHz, $CDCl_3$, 300 K) of compound **2**

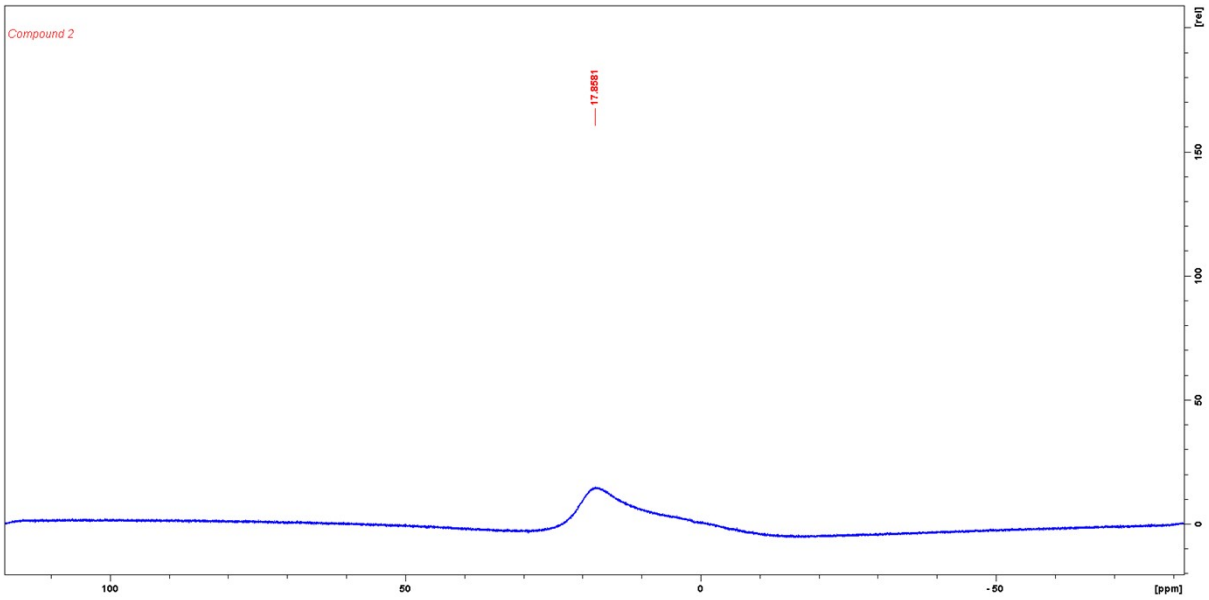

Figure S12. ^{1}H NMR (500.20 MHz, C_6D_6, 300 K) of compound **3**

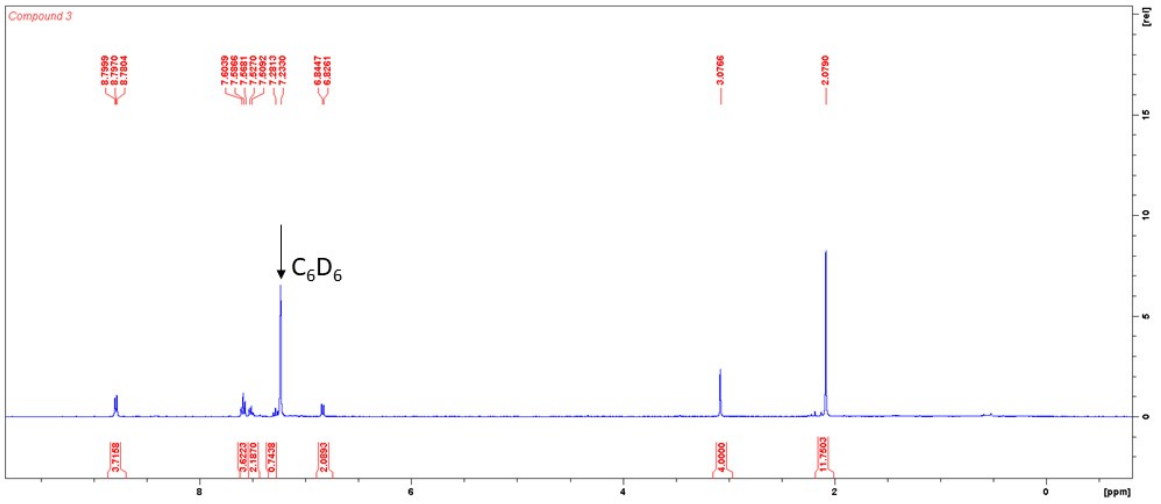

Figure S13. $^{13}C\{^{1}H\}$ NMR APT spectrum (125.78 MHz, C_6D_6, 300 K) of compound **3**

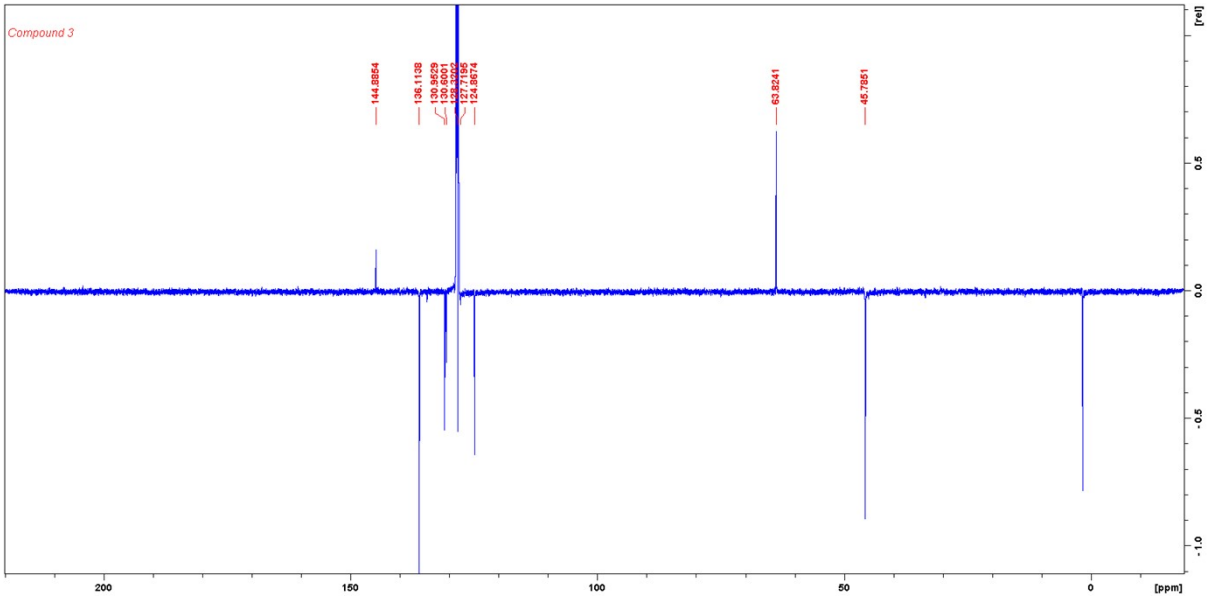

Figure S14. $^{11}B\{^{1}H\}$ NMR (160.49 MHz, C_6D_6, 300 K) of compound **3**

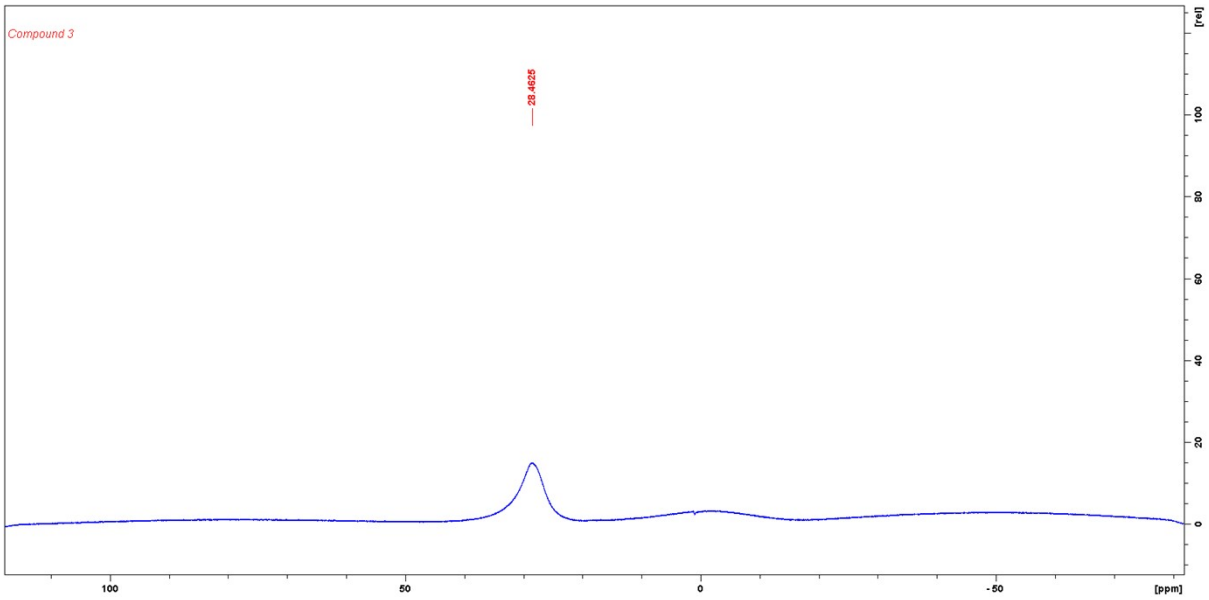

Figure S15. ^{1}H NMR (500.20 MHz, C_6D_6, 300 K) of compound **4**

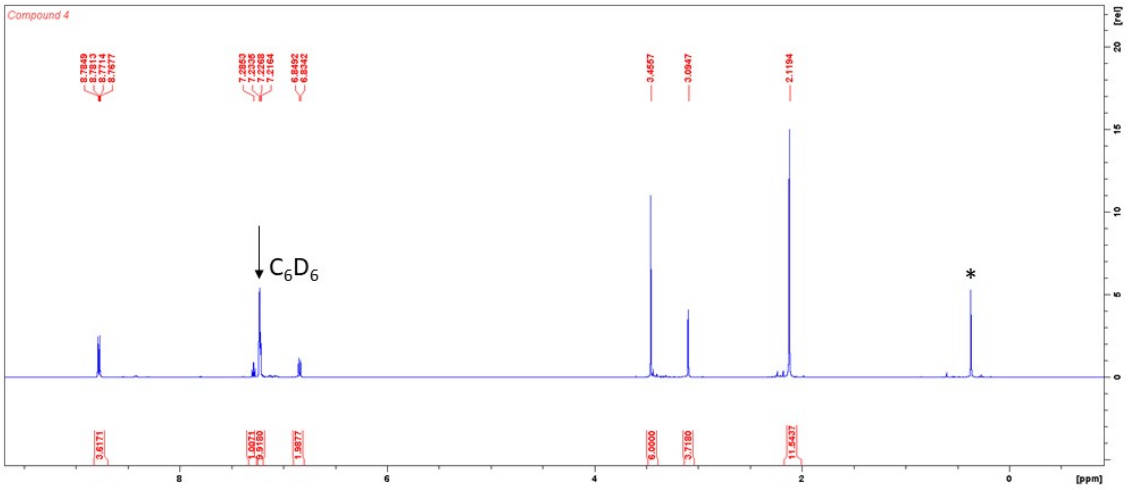

* peak of silicon grease

Figure S16. $^{13}C\{^{1}H\}$ NMR APT spectrum (125.78 MHz, C_6D_6, 300 K) of compound **4**

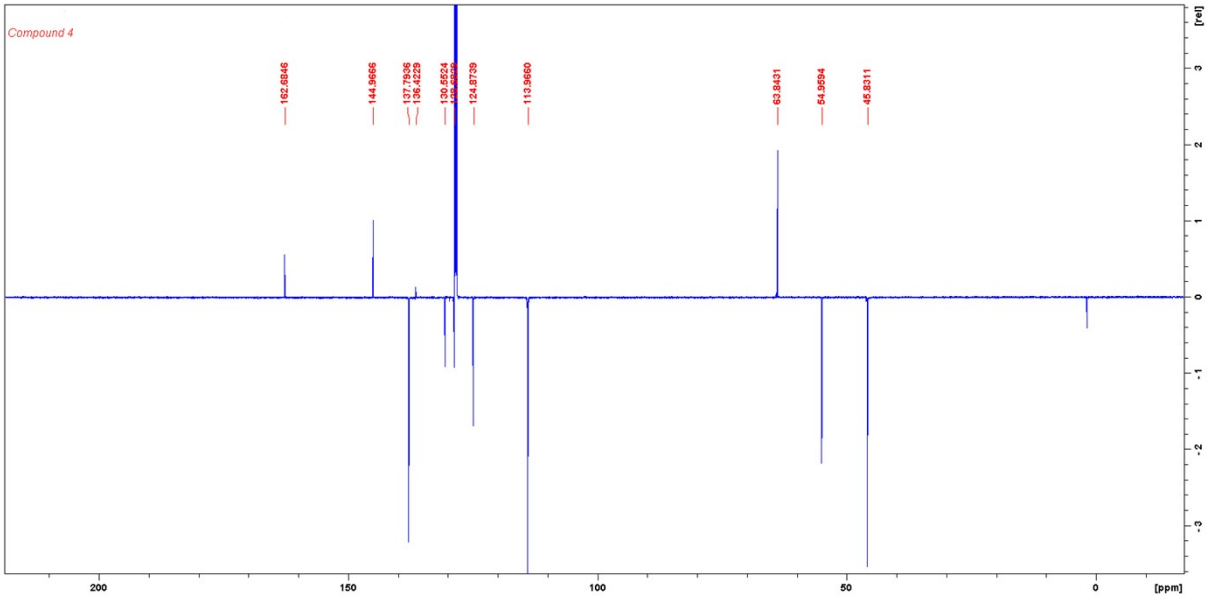

Figure S17. $^{11}B\{^{1}H\}$ NMR (160.49 MHz, C_6D_6, 300 K) of compound **4**

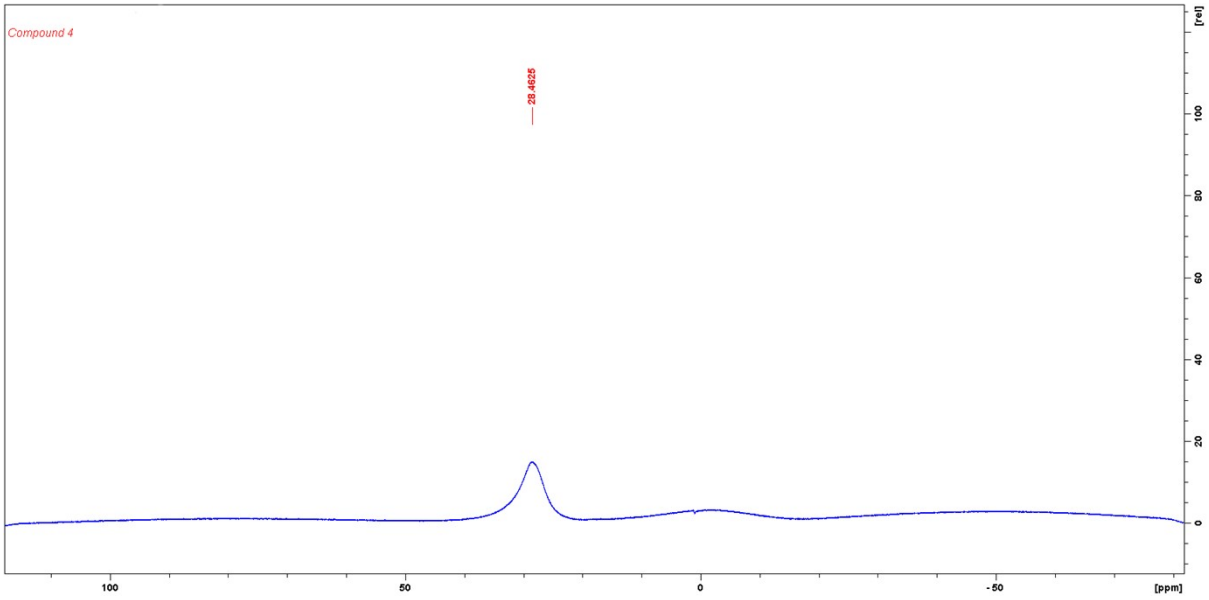

Figure S18. ^{1}H NMR (500.20 MHz, C_6D_6, 300 K) of compound **5**

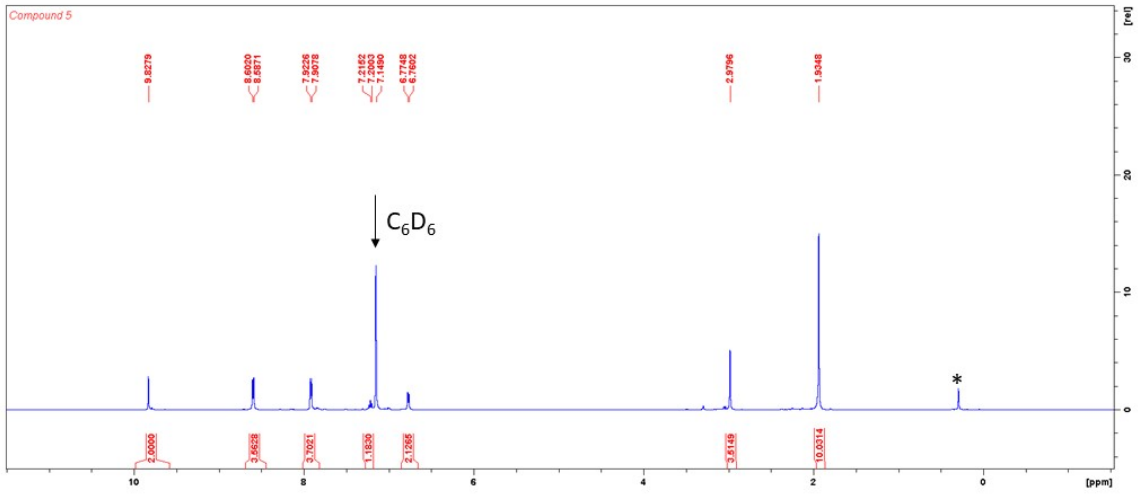

* peak of silicon grease

Figure S19. $^{13}C\{^{1}H\}$ NMR APT spectrum (125.78 MHz, C_6D_6, 300 K) of compound **5**

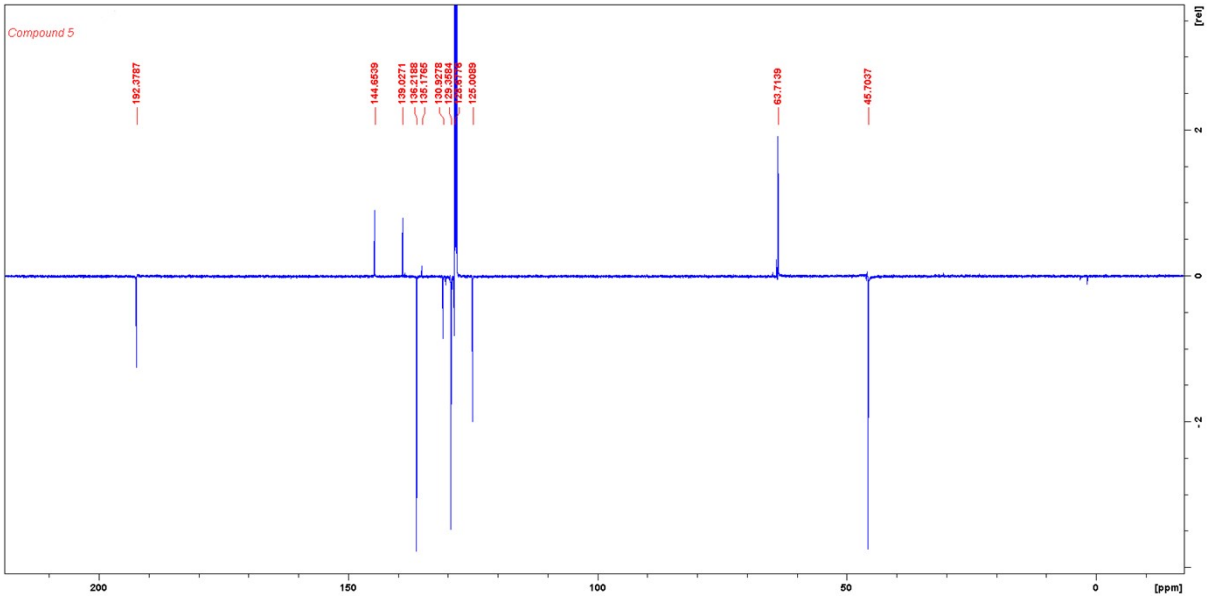

Figure S20. $^{11}B\{^{1}H\}$ NMR (160.49 MHz, C_6D_6, 300 K) of compound **5**

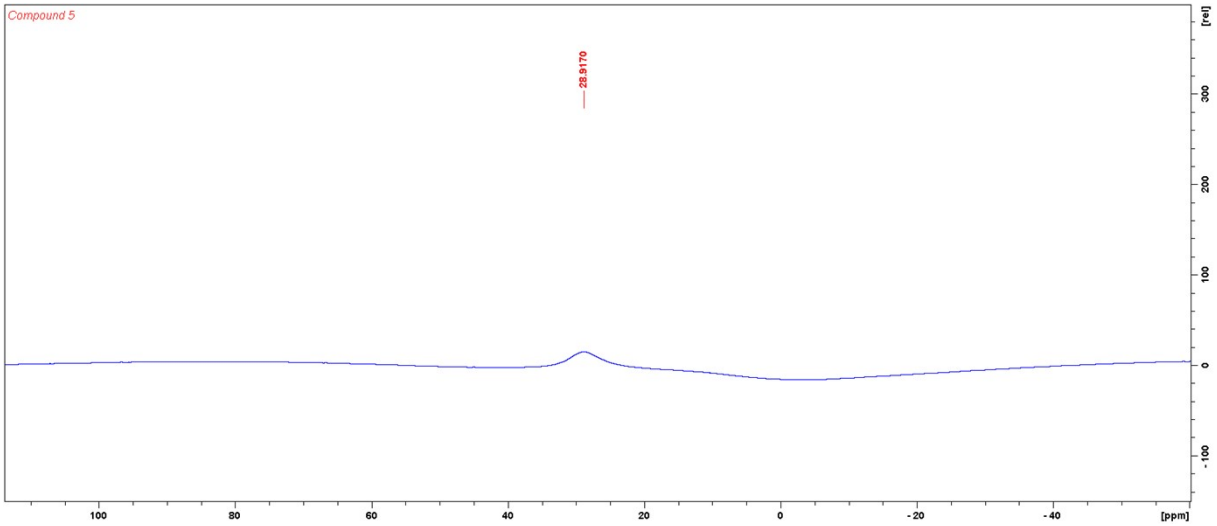

Figure S21. $^{13}C\{^{1}H\}$ NMR spectrum (125.78 MHz, C_6D_6, 300 K) of dissolved thin layer of GBO **5** spin coated at 500 rpm

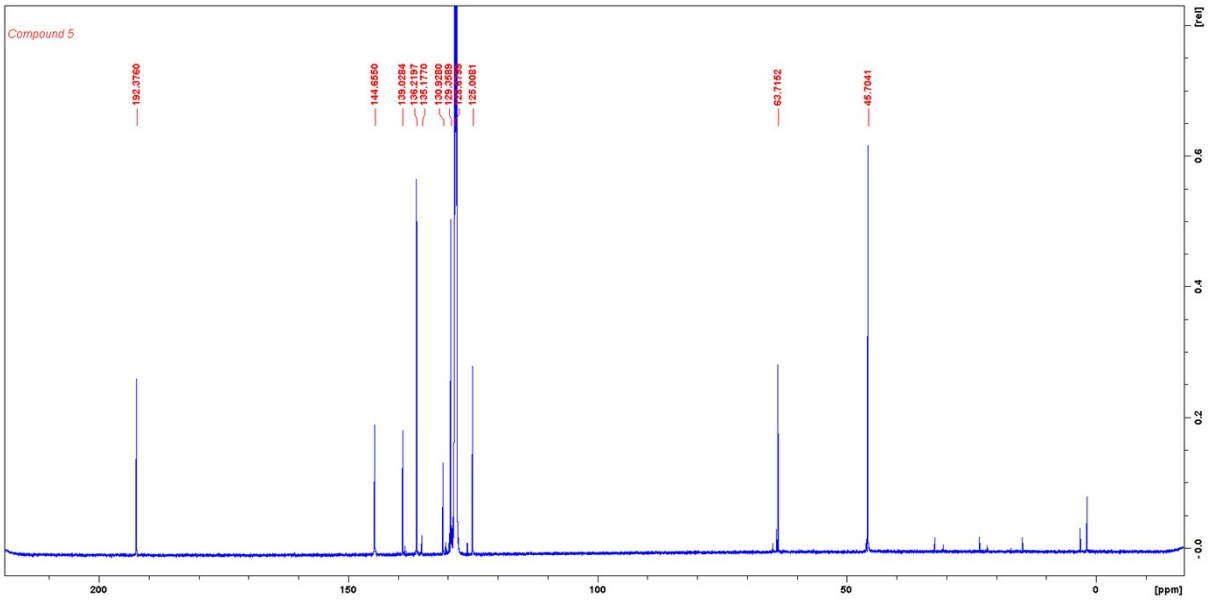

..

Figure S22. ^{1}H NMR (500.20 MHz, C_6D_6, 300 K) of compound **6**

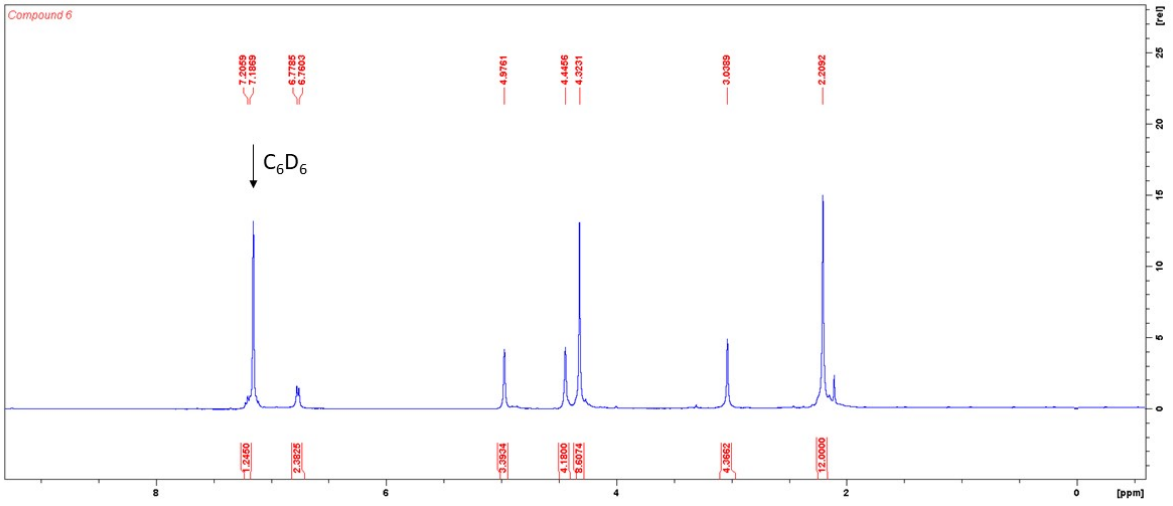

Figure S23. $^{13}C\{^{1}H\}$ NMR APT spectrum (125.78 MHz, C_6D_6, 300 K) of compound **6**

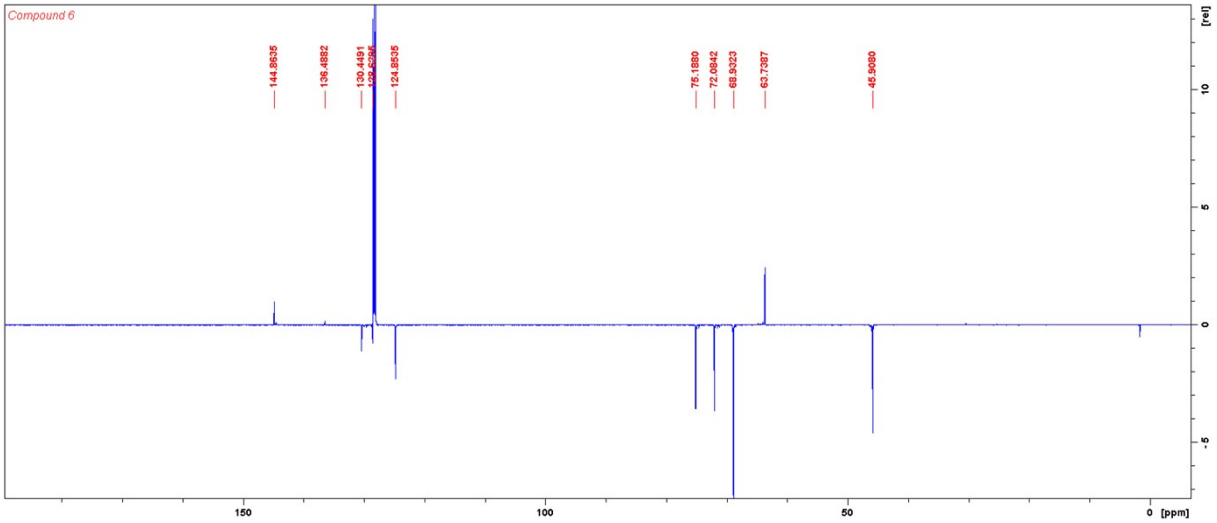

Figure S24. $^{11}B\{^{1}H\}$ NMR (160.49 MHz, C_6D_6, 300 K) of compound **6**

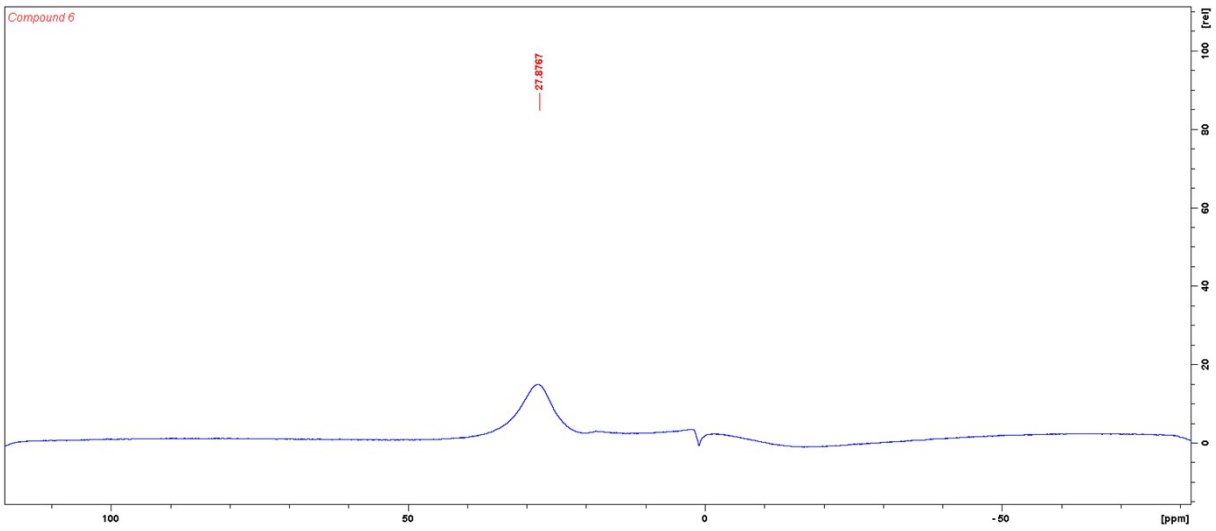

Figure S25. TGA analysis of GBO **2**. The black line shows the dependence of the relative sample weight on the temperature. The red line shows the dependence of the rate of the change of the sample weight (derivate weight) on the temperature. The derivative thermal gravimetric (DTG) peaks are observed at 100 and 250 °C.

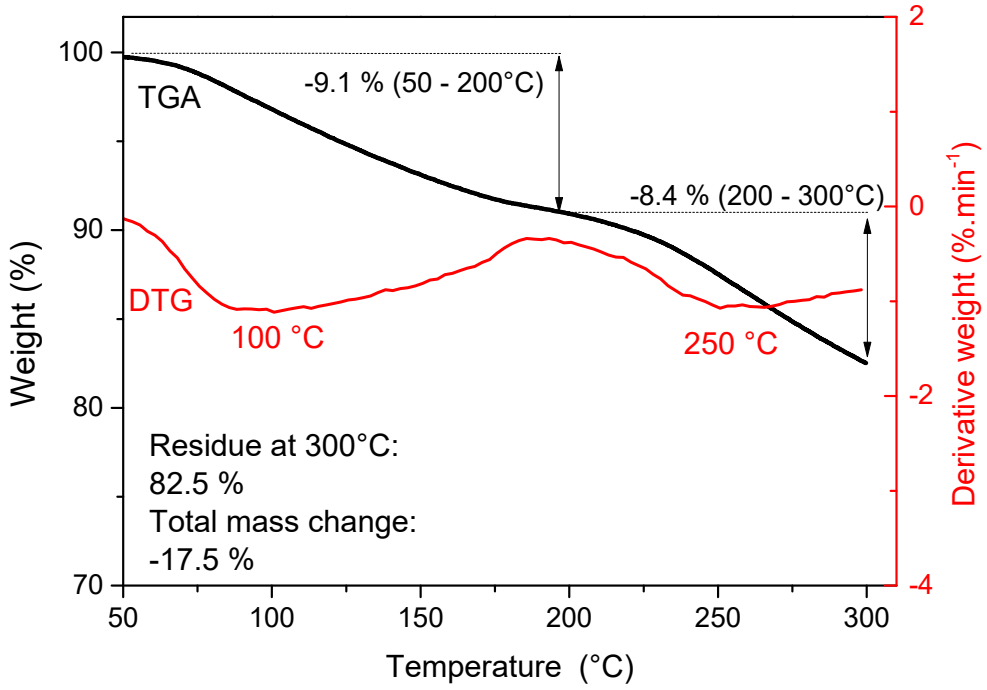

Figure S26. TGA analysis of GBO **3**. The black line shows the dependence of the relative sample weight on the temperature. The red line shows the dependence of the rate of the change of the sample weight (derivate weight) on the temperature. The derivative thermal gravimetric (DTG) peaks are observed at 126 and 174 °C.

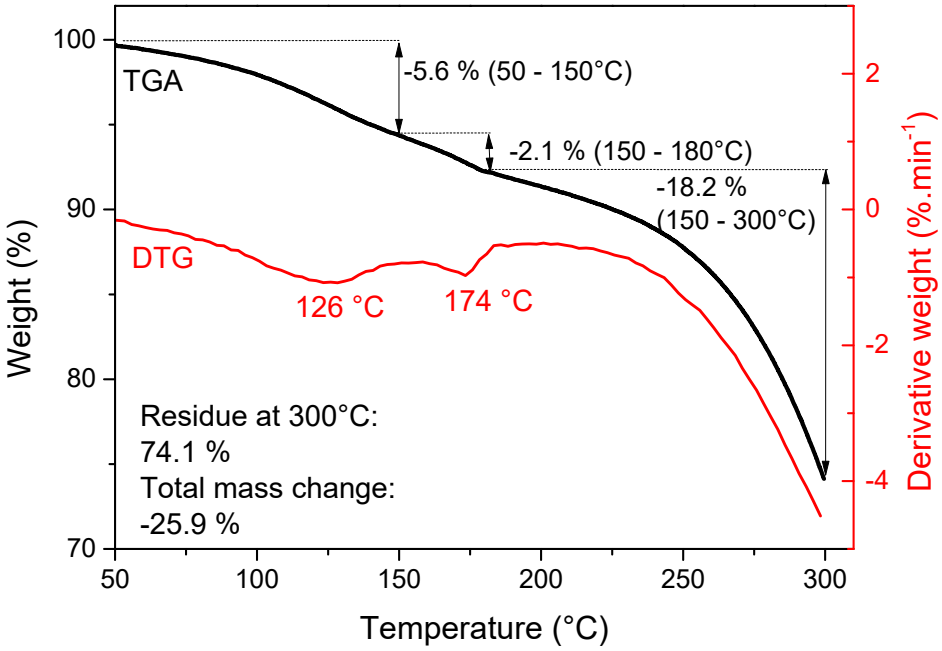

Figure S27. TGA analysis of GBO **4**. The black line shows the dependence of the relative sample weight on the temperature. The red line shows the dependence of the rate of the change of the sample weight (derivate weight) on the temperature. The derivative thermal gravimetric (DTG) peaks are observed at 130 and 205 °C.

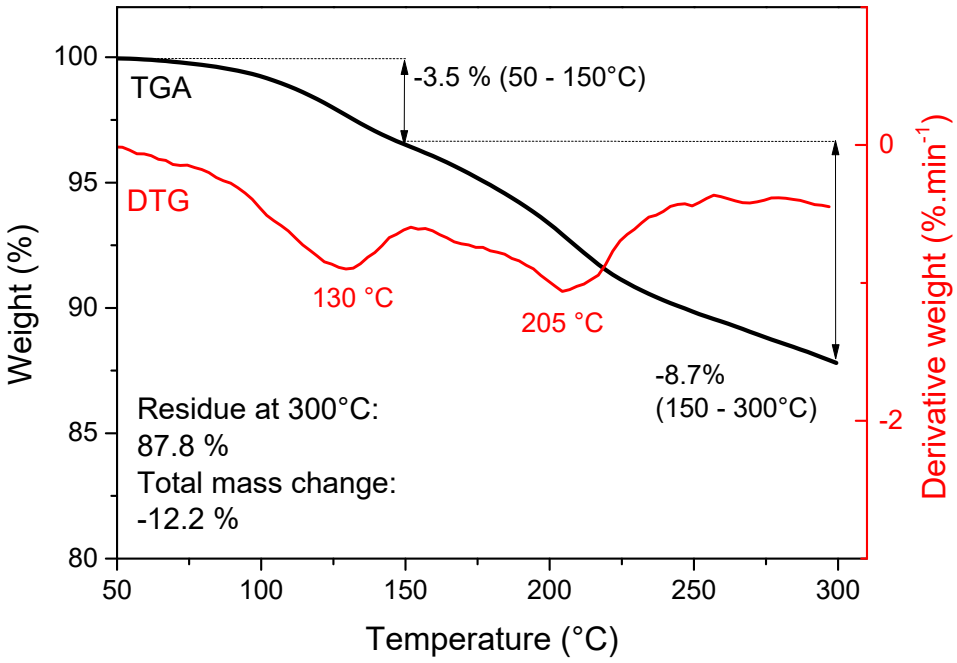

Figure S28. TGA analysis of GBO **5** measured a) under N_2 and b) under air atmosphere. The black line shows the dependence of the relative sample weight on the temperature. The red line shows the dependence of the rate of the change of the sample weight (derivate weight) on the temperature.

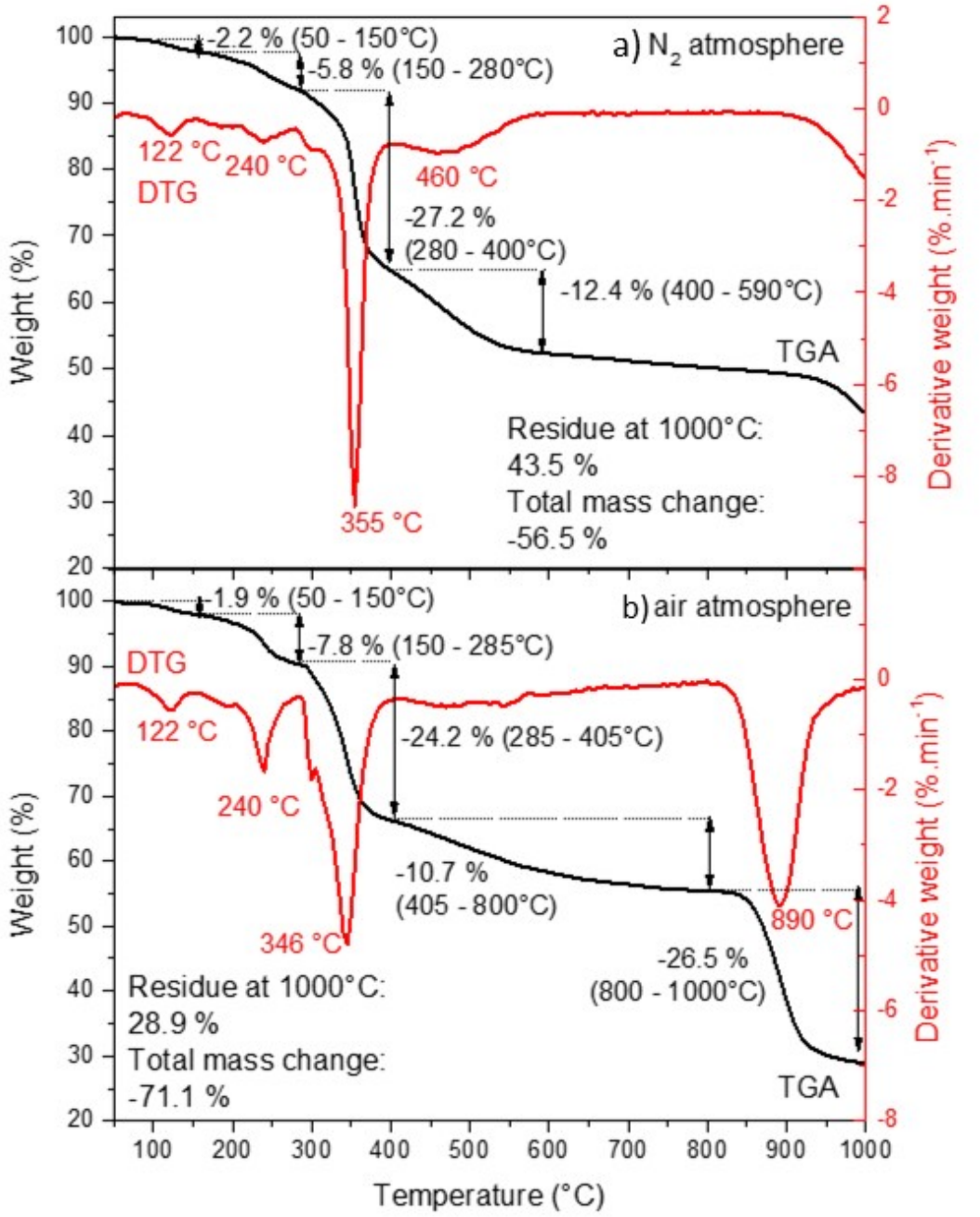

Figure S29. TGA analysis of GBO **6**. The black line shows the dependence of the relative sample weight on the temperature. The red line shows the dependence of the rate of the change of the sample weight (derivate weight) on the temperature. The derivative thermal gravimetric (DTG) peaks are observed at 83, 124, and 190 °C.

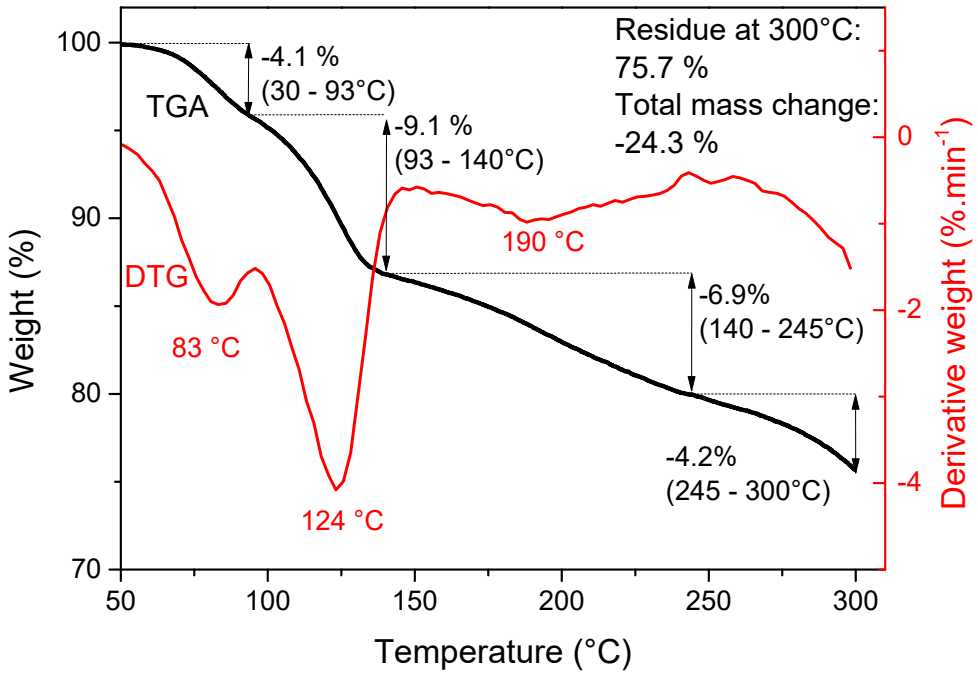

Figure S30. Mass spectrum (EI-MS) evolved gas from thermal decomposition of GBO **5** during thermal analysis. The maximum relative abundance (100%) is derived from the maximum peak m/z = 58, which corresponds to fragment Me_2NCH_2. The molecular ion peak has a value of m/z = 192, which corresponds to the molecular weight of ligand L (L is 2,6-$(Me_2NCH_2)_2C_6H_3$).

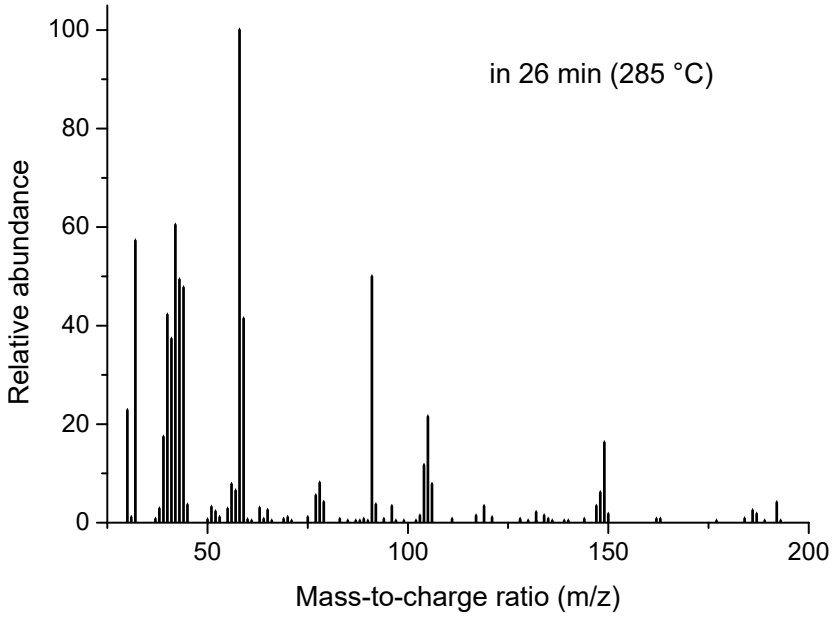

Figure S31. SEM image of the surface of spin-coated thin film of GBO **2** on silicon wafer

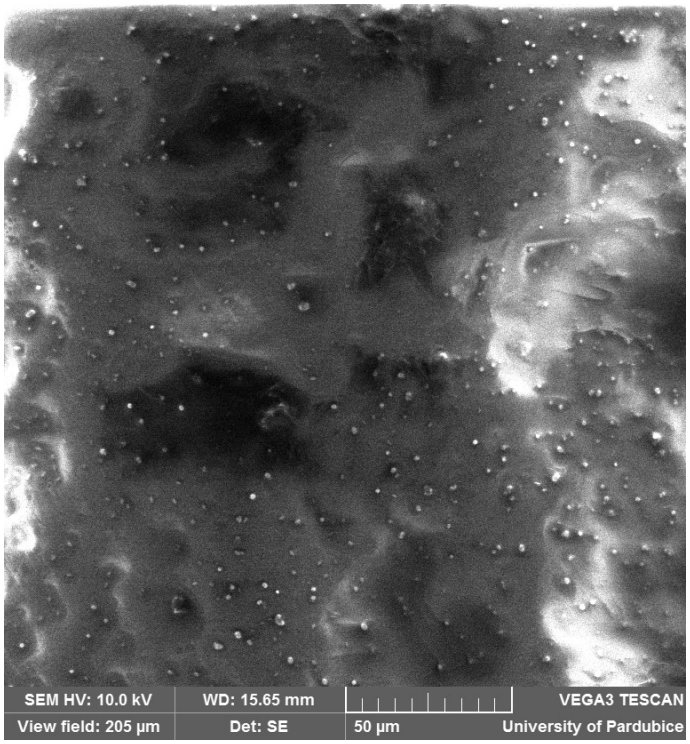

Figure S32. SEM image of the surface of spin-coated thin film of GBO **3** on silicon wafer

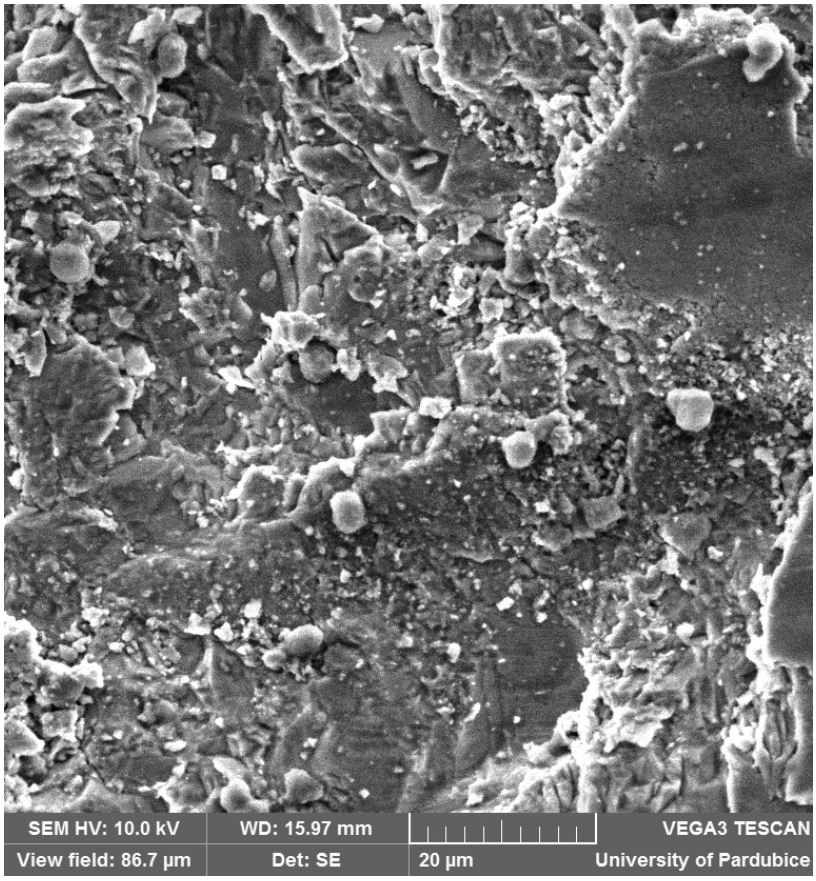

Figure S33. SEM image of the surface of spin-coated thin film of GBO **4** on silicon wafer

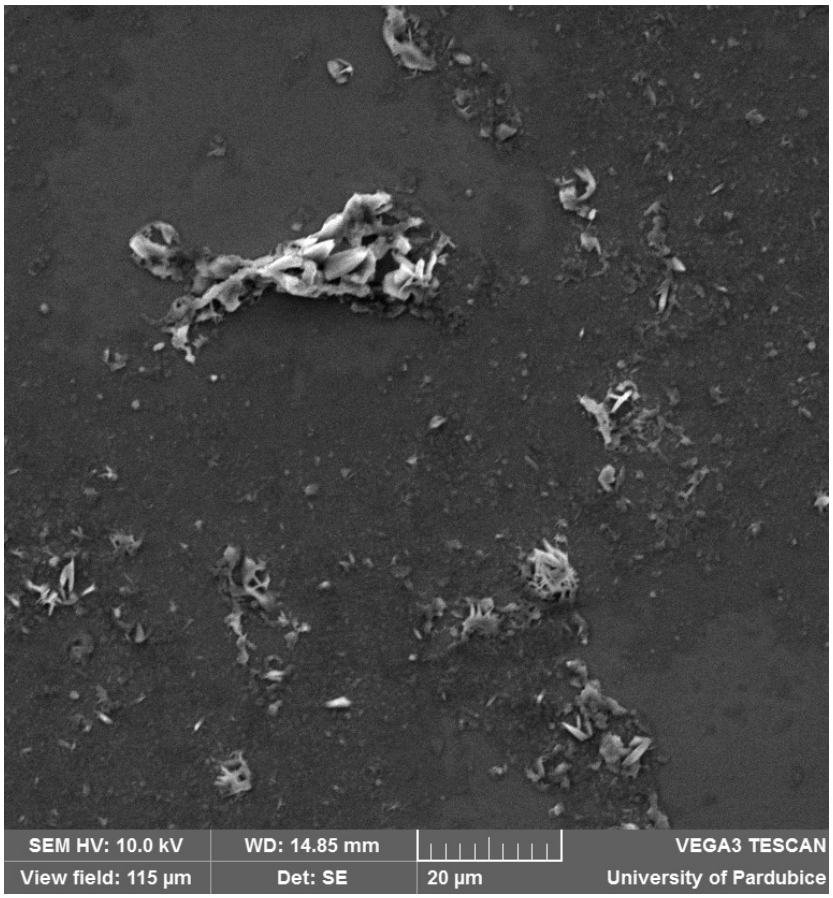

Figure S34. SEM image of the surface of spin-coated thin film of GBO **6** on silicon wafer

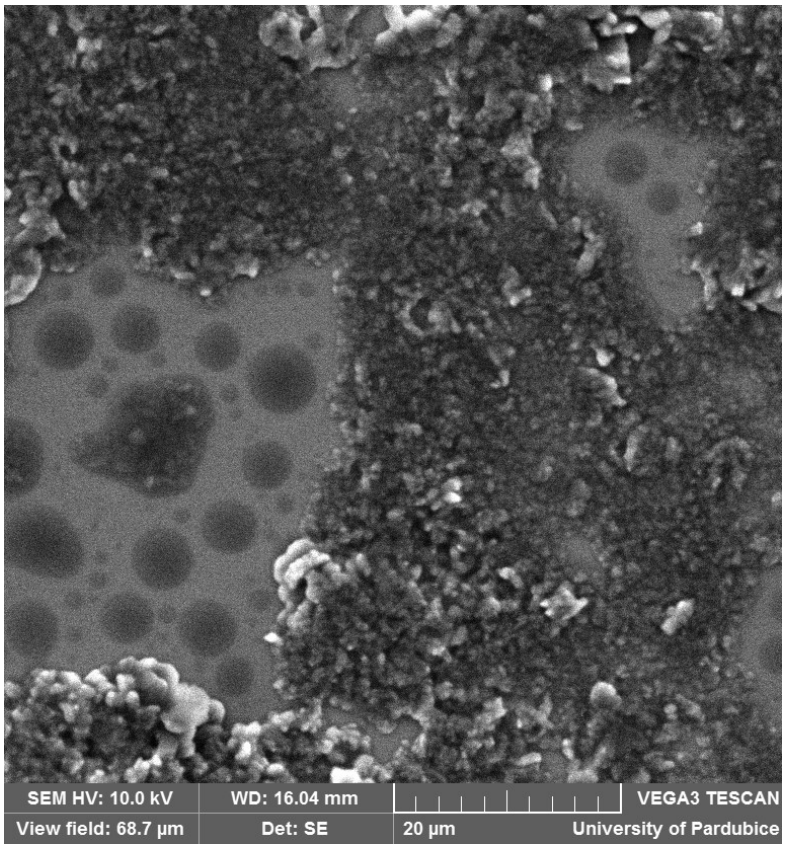

Figure S35. SEM image of the surface of spin-coated thin film of GBO **5** on silicon wafer

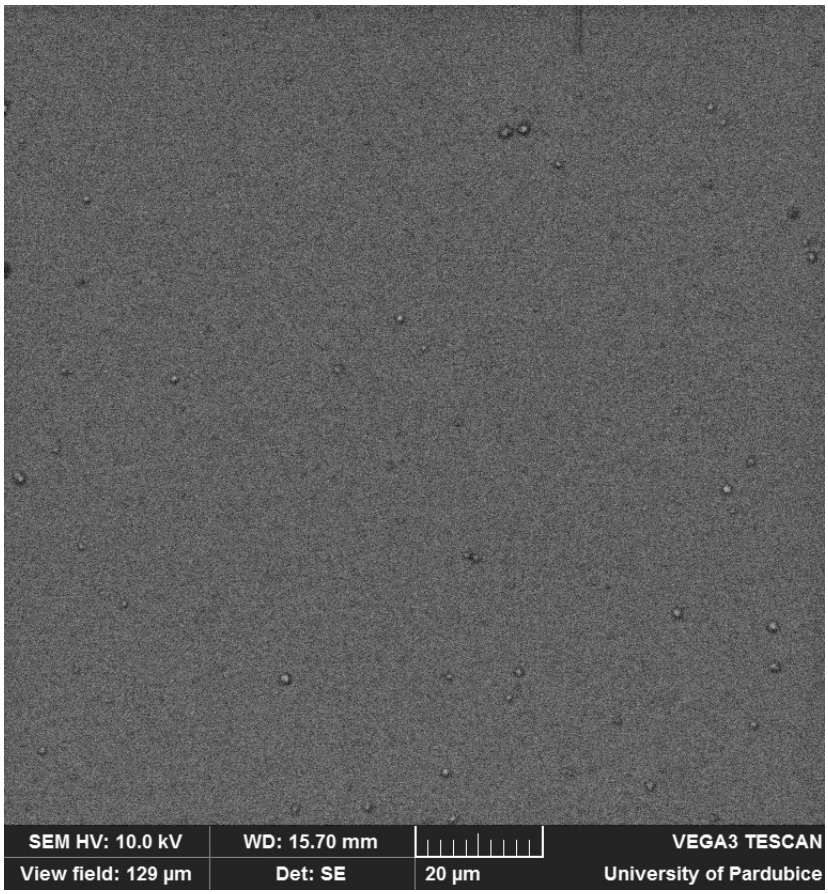

Figure S36. IR spectra of thin layers of **5** prepared by spin coating at SiO_2 (red) and Si wafer (green) using single-bounce diamond ATR. The IR spectrum of thin layer at Si wafer (purple) was also measured by transmission IR. The region of ν = 1300 – 1700 cm^{-1} is given only due to the absorption of the SiO_2 under the 1300 cm^{-1}.

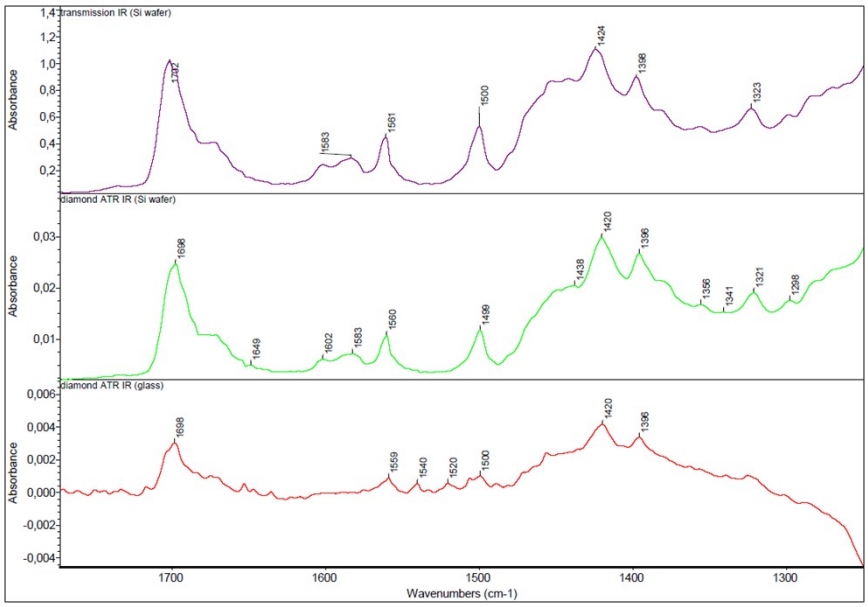

Figure S37. Typical dispersion of the refractive index of spin-coated thin film of GBO **5** on silicon wafer

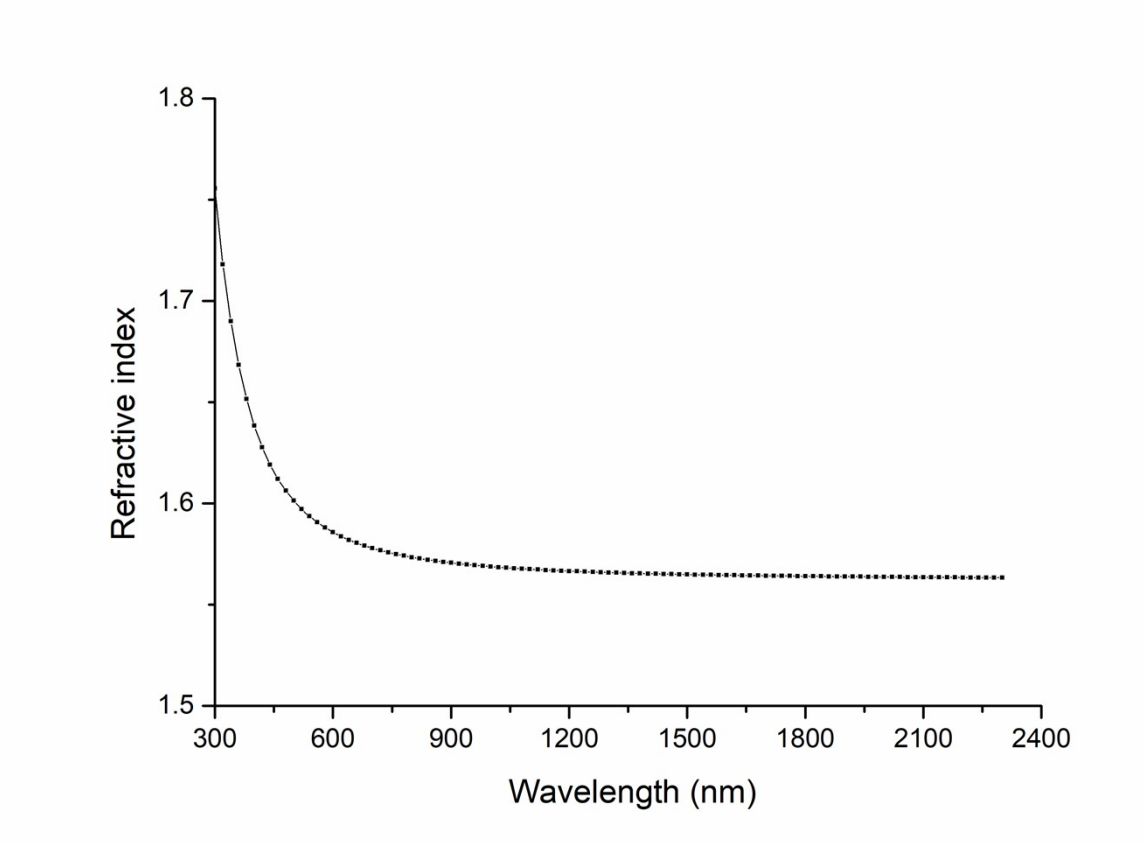

Figure S38. Spectral dependence of absorption coefficient in $(Khv)^{1/2}$ vs. hν coordinates for spin-coated thin films of GBO **5** on SiO_2.

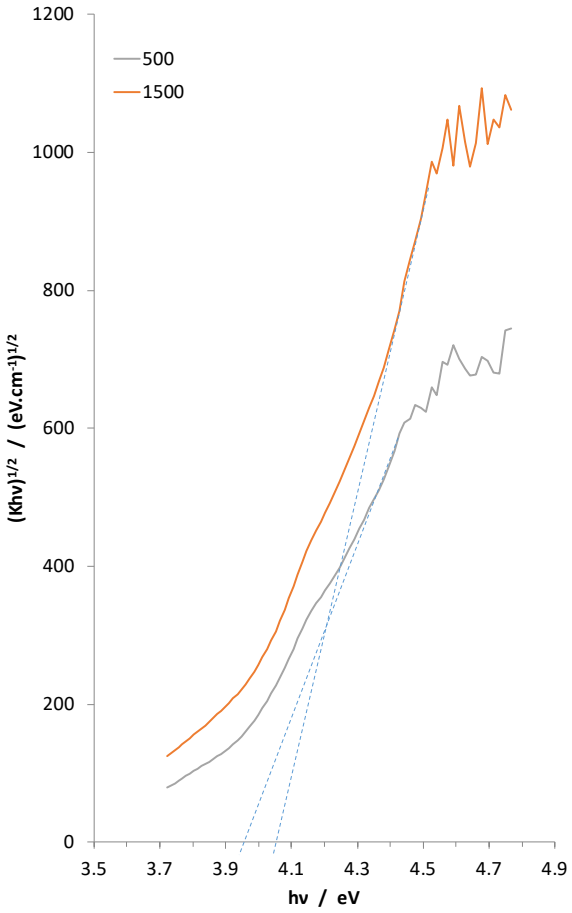

Figure S39. The arrangement of an experiment for measuring direct current conductivity of spin-coated thin films of GBO **5** on SiO_2.

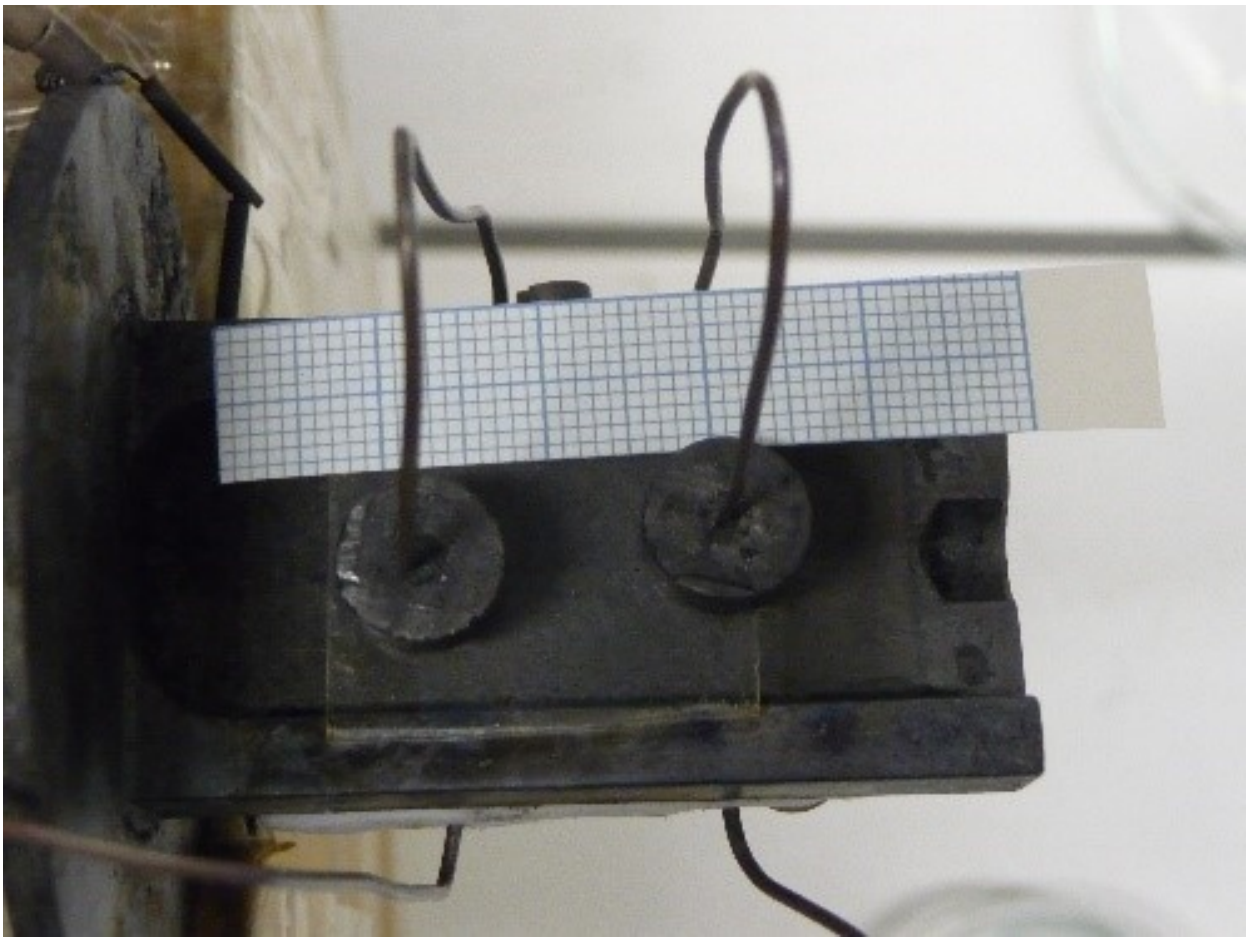

Figure S40. EDX spectrum of GBO **5** doped with 10 wt. % ErQ (a), and 10 wt. % $HoCl_3$ (b)

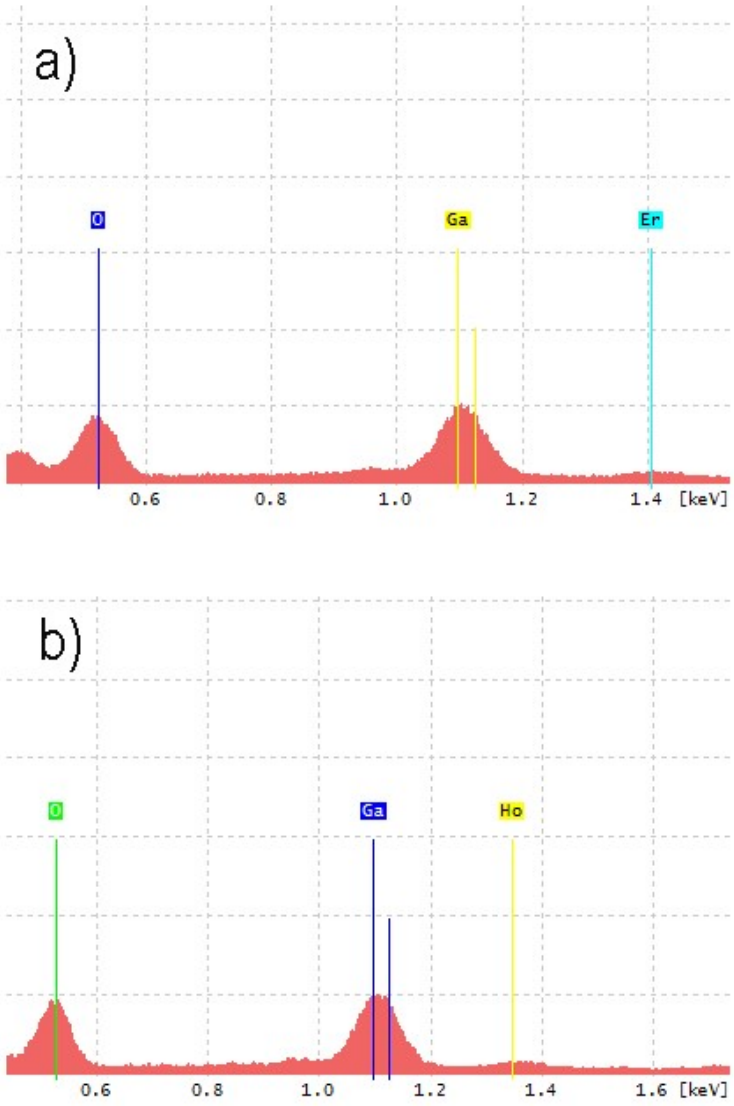

Figure S41. IR spectra of thin layers of doped GBO **5** prepared by spin coating on Si substrate a) GBO **5** + 1 wt. % $HoCl_3$, b) GBO **5** + 1 wt. % ErQ, c) GBO **5** + 10 wt. % $HoCl_3$, d) GBO **5** + 10 wt. % ErQ

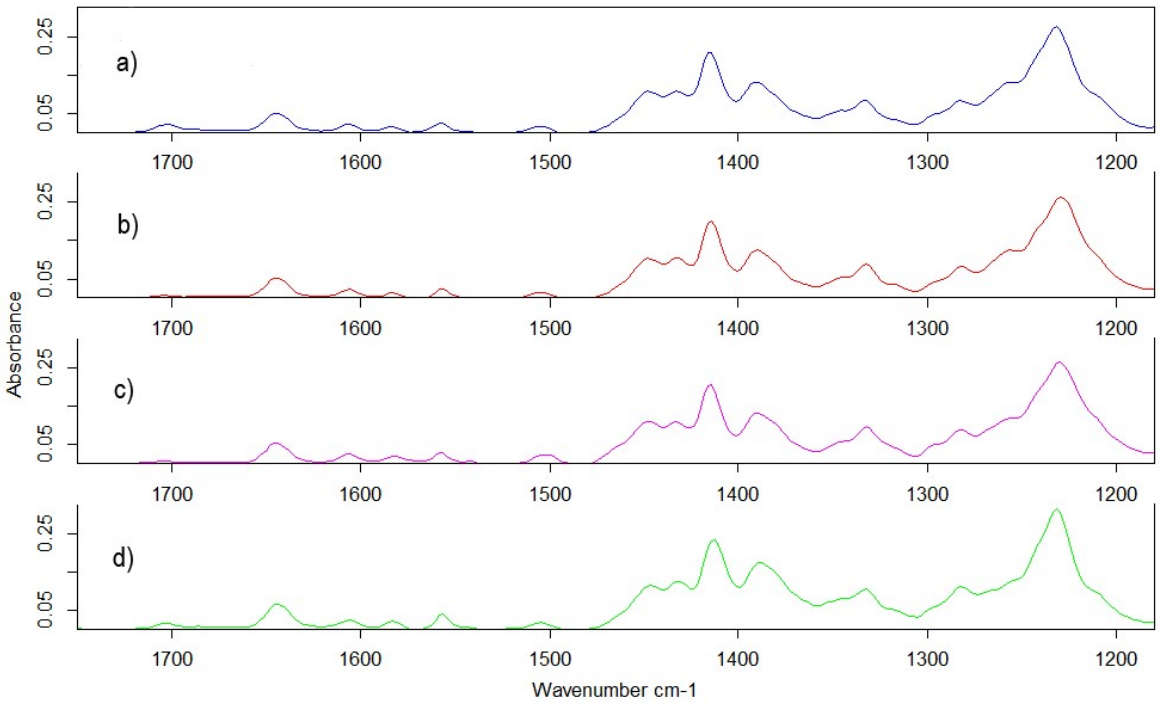

Figure S42. FT-IR spectra of original GBO **5,** thin layer of GBO **5** prepared by gravure printing technique at PET substrate, spectra of PET substrate and layer from ink without presence of GBO.

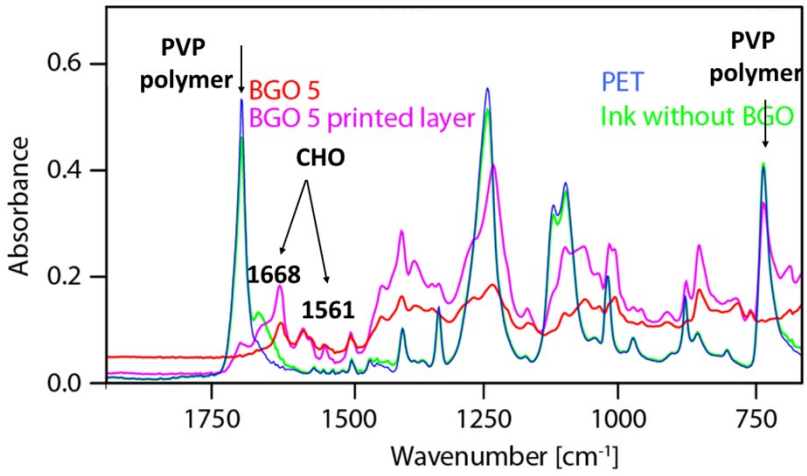

Figure S43. Photo of printed GBO **5** layers on PET substrate captured at highest angle of the reflection with black background.

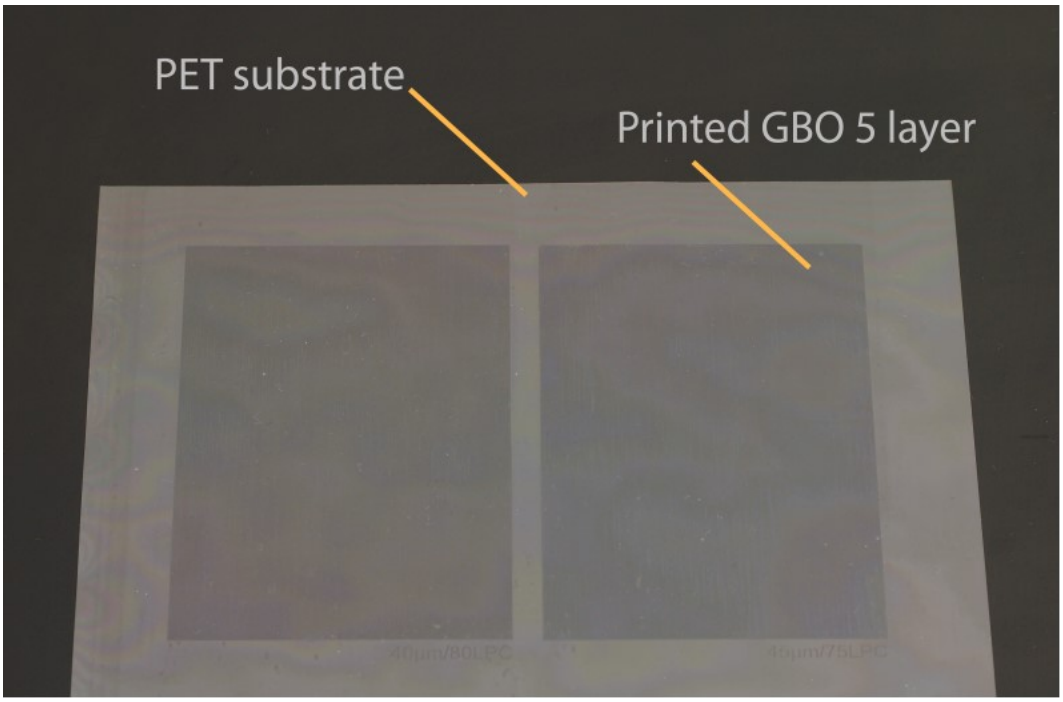

Figure S44. UV-VIS spectrum of GBO **6** in dichloromethane. Spectrum was measured in 1 cm quartz glass cuvete using StelarNet BLACK-Comet-SR spectrometer

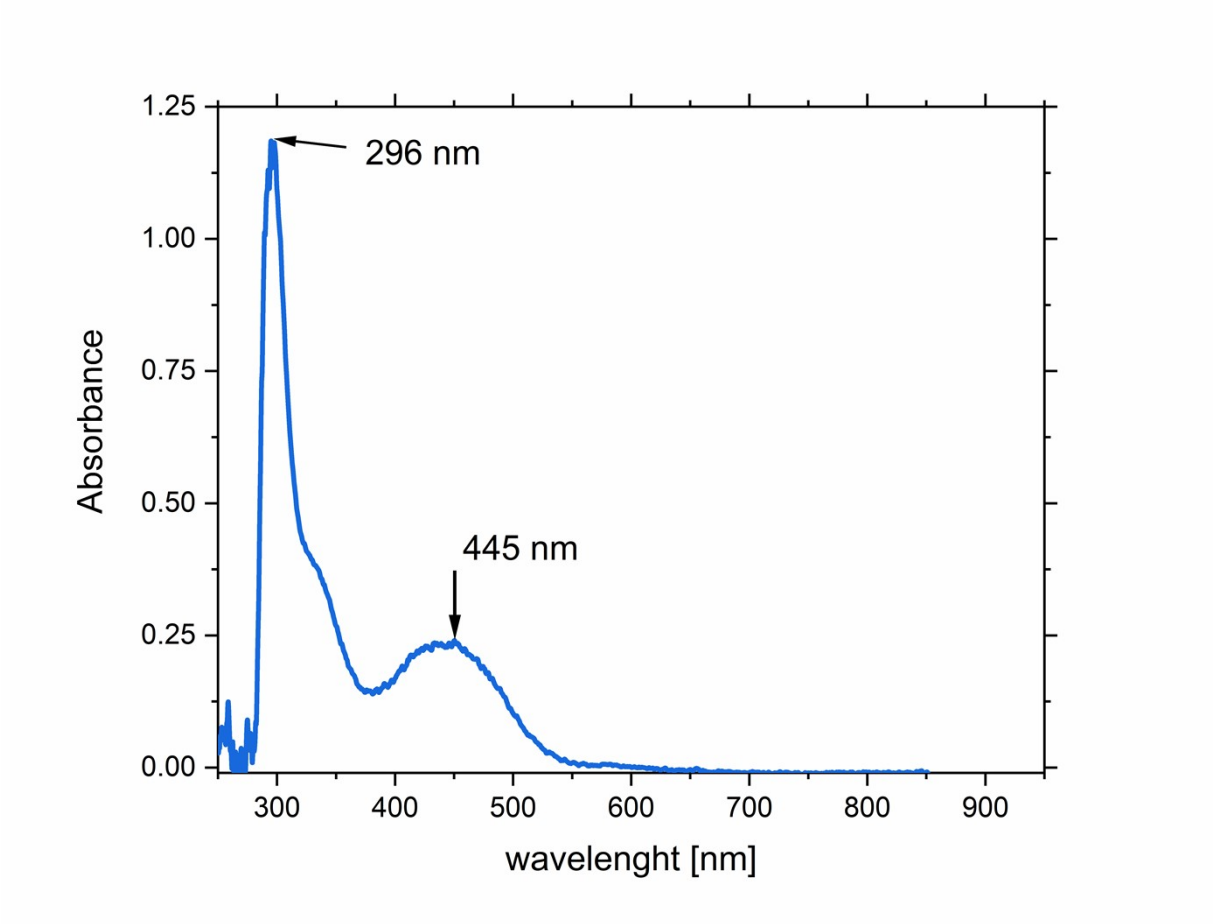

Table S1. Crystallographic details for **2**

Crystal data	
Chemical formula	$C_{48}H_{76}B_8Ga_4N_8O_{20}$
M_r	1450.52
Crystal system, space group	Monoclinic, $P2_1/c$
Temperature (K)	150
a, b, c (Å)	8.3230 (5), 17.5860 (12), 12.3120 (8)
β (°)	111.524 (5)
V (Å^3)	1676.42 (19)
Z	1
Radiation type	Mo $K\alpha$
μ (mm^{-1})	1.66
Crystal size (mm)	0.33 × 0.28 × 0.15
Data collection	
Diffractometer	Bruker Nonius KappaCCD area detector
Absorption correction	Multi-scan *SADABS2016*/2 - Bruker AXS area detector scaling and absorption correction
T_{min}, T_{max}	0.533, 0.746
No. of measured, independent and observed [$I > 2\sigma(I)$] reflections	13535, 3752, 2933
R_{int}	0.033
$(\sin \theta/\lambda)_{max}$ (Å^{-1})	0.650
Refinement	
$R[F^2 > 2\sigma(F^2)]$, $wR(F^2)$, S	0.032, 0.075, 1.07
No. of reflections	3752
No. of parameters	203
H-atom treatment	H-atom parameters constrained
$\Delta\rho_{max}$, $\Delta\rho_{min}$ (e Å^{-3})	0.79, −0.35

Computer programs: *COLLECT* (Hooft, 1998) and *DENZO* (Otwinowski & Minor, 1997), *COLLECT* and *DENZO*, *SIR92* (Altomare *et al.*, 1994), *SHELXL2017*/1 (Sheldrick, 2017), *PLATON* (Spek, 2003), *SHELXL97* (Sheldrick, 2008).

Table S2. Crystallographic details for **3**

Crystal data	
Chemical formula	$C_{24}H_{29}B_2GaN_2O_3$
M_r	484.83
Crystal system, space group	Monoclinic, *C*2/*c*
Temperature (K)	150
a, *b*, *c* (Å)	16.1481 (10), 18.3530 (9), 8.8820 (14)
β (°)	117.550 (4)
V (Å^3)	2333.8 (3)
Z	4
Radiation type	Mo *K*α
μ (mm^{-1})	1.21
Crystal size (mm)	0.43 × 0.34 × 0.18
Data collection	
Diffractometer	Bruker Nonius KappaCCD area detector
Absorption correction	Multi-scan *SADABS2016*/2 - Bruker AXS area detector scaling and absorption correction
T_{min}, T_{max}	0.591, 0.745
No. of measured, independent and observed [$I > 2\sigma(I)$] reflections	12927, 2670, 2426
R_{int}	0.025
$(\sin\theta/\lambda)_{max}$ (Å^{-1})	0.650
Refinement	
$R[F^2 > 2\sigma(F^2)]$, $wR(F^2)$, S	0.023, 0.064, 1.13
No. of reflections	2670
No. of parameters	147
H-atom treatment	H-atom parameters constrained
$\Delta\rho_{max}$, $\Delta\rho_{min}$ (e Å^{-3})	0.34, −0.42

Computer programs: *COLLECT* (Hooft, 1998) and *DENZO* (Otwinowski & Minor, 1997), *COLLECT* and *DENZO*, *SIR92* (Altomare *et al.*, 1994), *SHELXL2017*/1 (Sheldrick, 2017), *PLATON* (Spek, 2003), *SHELXL97* (Sheldrick, 2008).

Table S3. Crystallographic details for **4**

Crystal data	
Chemical formula	$C_{26}H_{33}B_2GaN_2O_5$
M_r	544.88

Crystal system, space group	Monoclinic, $P2_1/c$
Temperature (K)	150
a, b, c (Å)	9.2760 (2), 19.1690 (14), 15.055 (1)
β (°)	93.680 (4)
V (Å^3)	2671.4 (3)
Z	4
Radiation type	Mo $K\alpha$
μ (mm^{-1})	1.07
Crystal size (mm)	0.50 × 0.42 × 0.37
Data collection	
Diffractometer	Bruker Nonius KappaCCD area detector
Absorption correction	Integration Gaussian integration (Coppens, 1970)
T_{min}, T_{max}	0.635, 0.761
No. of measured, independent and observed [$I > 2\sigma(I)$] reflections	18118, 5703, 4865
R_{int}	0.026
$(\sin \theta/\lambda)_{max}$ (Å^{-1})	0.650
Refinement	
$R[F^2 > 2\sigma(F^2)]$, $wR(F^2)$, S	0.033, 0.086, 1.23
No. of reflections	5703
No. of parameters	325
H-atom treatment	H-atom parameters constrained
$\Delta\rho_{max}$, $\Delta\rho_{min}$ (e Å^{-3})	0.54, −0.42

Computer programs: *COLLECT* (Hooft, 1998) and *DENZO* (Otwinowski & Minor, 1997), *COLLECT* and *DENZO*, *SIR92* (Altomare *et al.*, 1994), *SHELXL2017*/1 (Sheldrick, 2017), *PLATON* (Spek, 2003), *SHELXL97* (Sheldrick, 2008).

Table S4. Crystallographic details for **5**

Crystal data	
Chemical formula	$C_{26}H_{29}B_2GaN_2O_5$
M_r	540.85
Crystal system, space group	Monoclinic, $C2/c$
Temperature (K)	150
a, b, c (Å)	17.1431 (10), 19.5340 (9), 9.2381 (14)

β (°)	121.931 (5)
V (Å^3)	2625.6 (3)
Z	4
Radiation type	Mo $K\alpha$
μ (mm^{-1})	1.09
Crystal size (mm)	0.36 × 0.24 × 0.20
Data collection	
Diffractometer	Bruker Nonius KappaCCD area detector
Absorption correction	Integration Gaussian integration (Coppens, 1970)
T_{min}, T_{max}	0.771, 0.855
No. of measured, independent and observed [$I > 2\sigma(I)$] reflections	12605, 2980, 2636
R_{int}	0.039
$(\sin \theta/\lambda)_{max}$ (Å^{-1})	0.650
Refinement	
$R[F^2 > 2\sigma(F^2)]$, $wR(F^2)$, S	0.029, 0.069, 1.12
No. of reflections	2980
No. of parameters	165
H-atom treatment	H-atom parameters constrained
$\Delta\rho_{max}$, $\Delta\rho_{min}$ (e Å^{-3})	0.40, −0.33

Computer programs: *COLLECT* (Hooft, 1998) and *DENZO* (Otwinowski & Minor, 1997), *COLLECT* and *DENZO*, *SIR92* (Altomare *et al.*, 1994), *SHELXL2017*/1 (Sheldrick, 2017), *PLATON* (Spek, 2003), *SHELXL97* (Sheldrick, 2008).

Table S5. Crystallographic details for **6**

Crystal data	
Chemical formula	$C_{31.99}H_{37}B_2Fe_2GaN_2O_3$
M_r	700.58
Crystal system, space group	Monoclinic, $P2_1/c$
Temperature (K)	150
a, b, c (Å)	12.371 (3), 17.560 (2), 13.898 (3)
β (°)	90.591 (15)
V (Å^3)	3019.0 (9)

Z	4
Radiation type	Mo $K\alpha$
μ (mm^{-1})	1.87
Crystal size (mm)	0.41 × 0.25 × 0.15
Data collection	
Diffractometer	Bruker Nonius KappaCCD area detector
Absorption correction	Integration Gaussian integration (Coppens, 1970)
T_{min}, T_{max}	0.539, 0.815
No. of measured, independent and observed [$I > 2\sigma(I)$] reflections	24882, 6890, 4528
R_{int}	0.102
(sin $\theta/\lambda)_{max}$ (Å^{-1})	0.650
Refinement	
$R[F^2 > 2\sigma(F^2)]$, $wR(F^2)$, S	0.070, 0.177, 1.06
No. of reflections	6890
No. of parameters	339
No. of restraints	940
H-atom treatment	H-atom parameters constrained $w = 1/[\sigma^2(F_o^2) + (0.0393P)^2 + 16.277P]$ where $P = (F_o^2 + 2F_c^2)/3$
$\Delta\rho_{max}$, $\Delta\rho_{min}$ (e Å^{-3})	1.52, −1.22

Computer programs: *COLLECT* (Hooft, 1998) and *DENZO* (Otwinowski & Minor, 1997), *COLLECT* and *DENZO*, *SIR92* (Altomare *et al.*, 1994), *SHELXL2017*/1 (Sheldrick, 2017), *PLATON* (Spek, 2003), *SHELXL97* (Sheldrick, 2008).

$R_{int} = \sum | F_o^2 - F_{o,mean}^2 | / \sum F_o^2$, GOF = $[\sum(w(F_o^2 - F_c^2)^2)/(N_{diffrs} - N_{params})]^{½}$ for all data, $R(F) = \sum | | F_o | - | F_c | | / \sum | F_o |$ for observed data, $wR(F^2) = [\sum(w(F_o^2 - F_c^2)^2)/(\sum w(F_o^2)^2)]^{½}$ for all data.

Table S6. Elemental composition of initial GBO **5** and thin GBO layer sputtered on glass slide (500 rpm)

Sample	Elemental analysis in at. %		
	C	H	N
GBO **5**	57.2	5.3	5.1
thin layer GBO after vacuum drying at 50°C	57.9	5.5	5.3

Literature

S1 a) R. Spotorno, M. Ostrowska, S. Delsante, U. Dahlmann, P. Piccardo, *Materials* **2020**, 13, 4702; b) M. M. El-Desoky, N. K. Wally, E. Sheha, B. M. Kamal, *J Mater Sci: Mater Electron* **2021**, 32, 3699–3712.

S2 a) V. V. Kurtskhaliya, A. V. Sarukhanishvili, T. S. Cheishvili, *Glass Phys. Chem.* **2002**, *28*, 184–188; b) B. Roling, A. Happe, K. Funke, M. D. Ingram, *Phys. Rev. Lett.* **1977**, *78*, 2160–2163.